Editors' Suggestion

Classification of topological insulators and superconductors out of equilibrium

Max McGinley and Nigel R. Cooper
T.C.M. Group, Cavendish Laboratory, University of Cambridge, JJ Thomson Avenue, Cambridge CB3 0HE, United Kingdom

(Received 2 November 2018; published 25 February 2019)

We establish the existence of a topological classification of many-particle quantum systems undergoing unitary time evolution. The classification naturally inherits phenomenology familiar from equilibrium—it is robust against disorder and interactions, and exhibits a nonequilibrium bulk-boundary correspondence, which connects bulk topological properties to the entanglement spectrum. We explicitly construct a nonequilibrium classification of noninteracting fermionic systems with nonspatial symmetries in all spatial dimensions (the 'tenfold way'), which differs from its equilibrium counterpart. Direct physical consequences of our classification are discussed, including important ramifications for the use of topological zero-energy bound states in quantum information technologies.

DOI: 10.1103/PhysRevB.99.075148

I. INTRODUCTION

Topology has become one of the most prevalent concepts in condensed matter physics. In mathematics, the objects of interest for topologists are structures that remain invariant under continuous deformations of the underlying system. Likewise, *physical* properties that do not change under continuous deformation of the underlying Hamiltonian are of interest in physics. In condensed matter, these topological properties are naturally robust to system imperfections and in some cases lead to accurately quantized responses, exemplified by the transverse conductance in the integer quantum Hall effect (IQHE) [1,2].

Classifying different phases of matter according to their topological properties is one of the key aims of this field. Roughly speaking, gapped systems belong to different topological phases when their Hamiltonians cannot be continuously connected without meeting some topological quantum phase transition [3]: a phase transition at zero temperature that is not characterized by spontaneous symmetry breaking [4]. These topological phases are typically understood to be equilibrium (zero-temperature) properties of the Hamiltonian, which itself may be restricted by the symmetries of the system [5].

In this paper, rather than characterizing ground states of Hamiltonians, we ask whether there is a topological classification of nonequilibrium states $|\Psi(t)\rangle$ resulting from time evolution under Hamiltonians with certain symmetries. We answer this question in the affirmative by developing a formalism for classifying wave functions which naturally generalizes the more familiar equilibrium classification. When applied to many-body systems undergoing unitary time evolution, this nonequilibrium topological classification emerges, which generally differs from that in equilibrium. The classification is relevant in physical settings where the Hamiltonian varies in time, e.g., through a deliberate quench or in the presence of random noise.

We explicitly realize this nonequilibrium classification by building on the understanding of topology in equilibrium. Indeed many of the current theoretically [6–10] and experimentally [11–13] known topological phases of matter can be understood through unifying perspectives. One key feature common to many of these phases is the presence of symmetries: Although two systems could in general be continuously connected, they may be disconnected in the subspace of states which respect certain symmetries—such systems constitute the symmetry-protected topological (SPT) and symmetry-enriched topological (SET) phases [5]. One important subset of SPT phases is the wide range of topological insulators and superconductors, which can be described by Hamiltonians that are quadratic in fermionic creation and annihilation operators (including mean-field Bogoliubov-de Gennes Hamiltonians) and have nonspatial symmetries. The equilibrium topology of these systems has been classified under the 'tenfold way' [3,14–16].

Access to coherent dynamics in cold atom experiments [17] has motivated recent studies of nonequilibrium physics in topological insulators and superconductors [18–23]. A key aspect of these studies is the behavior of topological bulk indices after a quench between Hamiltonians. In 2D Chern insulators (lattice analogues of the IQHE), it was shown that the relevant topological index (the Chern number) is preserved in time. However in Ref. [24] we demonstrated that in certain 1D systems, topological properties of symmetry-protected states can change out of equilibrium, even if the Hamiltonian never breaks the symmetries required to stabilize the phase in equilibrium.

The nonequilibrium classification which we construct in this paper unifies these previous results and establishes a universal phenomenology which can be applied to any isolated quantum system. We explicitly derive the nonequilibrium analog of the 'tenfold way,' describing topological insulators and superconductors in arbitrary spatial dimension (Table II). Specifically, given the spatial dimension and the set of symmetries possessed by the initial state and governing Hamiltonian, we provide an Abelian group, the elements of which represent states that remain topologically inequivalent after time evolution. The classification naturally pertains to physical properties that are robust to disorder and interactions, and exhibits a bulk-boundary correspondence. As a first direct

application of our results, we find that the classification can be used to predict instabilities of topological edge (Majorana) zero modes to decoherence from an external fluctuating perturbation. We postulate that this connection between the preservation (destruction) of bulk topology in our nonequilibrium topological classification and the (lack of) robustness of edge modes to symmetry-respecting temporal fluctuations should hold generally.

We note that other topological aspects of nonequilibrium dynamics have been discussed in recent works. One direction concerns 'Floquet-SPTs' [25–28], wherein the periodic micromotion of periodically driven systems is characterized. A rather striking result in that context is the emergence of 'anomalous' topologically protected edge modes which have no equilibrium analog, in that their presence cannot be deduced from static properties of the Floquet Hamiltonian [29,30]. In a similar light, we demonstrate that a time-evolving wave function can possess robust topological properties even if the Hamiltonian which governs its dynamics is itself trivial, which further highlights the distinction between topology in and out of equilibrium. (The connections between Floquet-SPT order and the results of our work are discussed in Sec. VII.)

Separately, recent studies on noninteracting fermions [31–34] have demonstrated that static topological phases can be detected via dynamics. These characterizations of the full wave-function trajectory after a quench, which can be measured via Bloch state tomography, are different from our nonequilibrium classification: They provide information about the Hamiltonian governing time evolution, rather than the wave function itself, and these protocols require translationally invariant, noninteracting systems.

Finally, there has recently been much attention focused on the topological properties of systems which can be described with effective non-Hermitian Hamiltonians [35–38], which are intrinsically out of equilibrium. A complete treatment of the effects of non-Hermiticity on the topology of a time-evolving wave function is outside the scope of this work, however analogous results should be obtainable for such systems.

Our paper is structured as follows: In Sec. II, we review the concept of 'dynamically-induced symmetry breaking' [24]—the observation that unitary time evolution can break the symmetries of the wave function even if the Hamiltonian respects the symmetries at all times. We then discuss how pure nonequilibrium states can be topologically classified in Sec. III and go on to derive this classification for free fermion systems with nonspatial symmetries in Sec. IV. Our classification is formulated such that it encapsulates all features familiar from equilibrium systems, which naturally leads to a nonequilibrium bulk-boundary correspondence that we develop in Sec. V. We then discuss direct physical consequences of our results in Sec. VI, before describing the relationships between our results and those found for Floquet systems in Sec. VII. We finally conclude in Sec. VIII.

II. SYMMETRY OF THE TIME-EVOLVED STATE

We are concerned with the topological properties of many-body states after generic unitary time evolution. Of central importance to topological properties in general is the impact of symmetry constraints. These symmetries are imposed at the level of the microscopic Hamiltonian in question. However, the many-body states which we consider are far from equilibrium, and so we must be careful to distinguish symmetry properties of the post-quench state and the Hamiltonian. We have established this relationship in Ref. [24]; we review the results here.

The quench protocol which we will refer to in this paper is highly general: The system starts in the ground state of some initial Hamiltonian $\hat{\mathcal{H}}^{\mathrm{i}}$ at time $t = 0$ and evolves under some final Hamiltonian $\hat{\mathcal{H}}^{\mathrm{f}}(t)$ which may itself vary in time. We then consider the properties of the state at some final time t_{f}.

If a symmetry is present in the initial Hamiltonian, then there exists some symmetry operator $\hat{\mathcal{O}}$ which commutes with $\hat{\mathcal{H}}^{\mathrm{i}}$. By Wigner's theorem, the operator $\hat{\mathcal{O}}$ can be unitary or antiunitary, i.e., $\hat{\mathcal{O}}i\hat{\mathcal{O}}^{-1} = \pm i$. Now, if the symmetry is not spontaneously broken, then the ground state of $\hat{\mathcal{H}}^{\mathrm{i}}$ (which we call $|\Psi_0\rangle$) also respects this symmetry, in the sense that the pure density matrix $\hat{\varrho}_0 := |\Psi_0\rangle\langle\Psi_0|$ satisfies $[\hat{\mathcal{O}}, \hat{\varrho}_0] = 0$. Note that we work with density matrices for convenience, but understand that they always represent a single pure wave function.

The state evolves as $|\Psi(t)\rangle = \hat{\mathcal{U}}(t)|\Psi(0)\rangle$, where $\hat{\mathcal{U}}(t) = \mathcal{T}\exp(-i\int_0^{t_{\mathrm{f}}} dt'\hat{\mathcal{H}}^{\mathrm{f}}(t'))$ is the time evolution operator ($\mathcal{T}$ denotes time ordering). Thus the density matrix after the full quench is $\hat{\varrho}(t_{\mathrm{f}}) = \hat{\mathcal{U}}(t_{\mathrm{f}})\hat{\varrho}_0\hat{\mathcal{U}}(t_{\mathrm{f}})^{\dagger}$. To determine whether the symmetry $\hat{\mathcal{O}}$ is respected by the time-evolved state, we compute $[\hat{\mathcal{O}}, \hat{\varrho}(t_{\mathrm{f}})]$, which will be zero if the symmetry is respected and nonzero otherwise.

If the final Hamiltonian $\hat{\mathcal{H}}^{\mathrm{f}}(t)$ does not commute with $\hat{\mathcal{O}}$, then the state will also not respect the symmetry—this we call explicit symmetry breaking. However, even if $\hat{\mathcal{H}}^{\mathrm{f}}(t)$ satisfies the symmetry at all times, the state will not be symmetric ($[\hat{\mathcal{O}}, \hat{\varrho}(t_{\mathrm{f}})] \neq 0$) if $\hat{\mathcal{O}}$ is an antiunitary operator—this we call dynamically induced symmetry breaking. One can see this as the factor of i in the exponent of $\hat{\mathcal{U}}(t)$ is not invariant under antiunitary operations [24].

It is therefore possible for the symmetry properties of the state and Hamiltonian to deviate out of equilibrium. This dynamically induced symmetry breaking has profound consequences for topology out of equilibrium.

Although we do not do so here, one could also consider quench protocols in which the final Hamiltonian is non-Hermitian, which captures certain gain and/or loss processes. In doing so, one must be careful to consider the relationship between symmetries of the initial state and the non-Hermitian Hamiltonian, the latter of which can have a more general set of symmetries [39]. Note, however, that this work is concerned with properties of the instantaneous wave function rather than the spectrum of the Hamiltonian, in contrast to previous studies of non-Hermitian topology [35–38].

III. DEFINING TOPOLOGY OUT OF EQUILIBRIUM

The topology of gapped short-ranged entangled (SRE) systems at zero temperature is a well-defined concept. Under a particular set of symmetry constraints, one constructs a set of topological *phases*, defined such that Hamiltonians which belong to different phases cannot be continuously deformed between each other without breaking the symmetry

constraints or crossing some topological quantum phase transition. In the majority of this paper, we are concerned with topological insulators under the 'tenfold way' (see Sec. IV), where the scope of 'continuous deformations' is rather broad. In particular, we are permitted to add trivial bands to a system, which for example excludes Hopf insulators [40] from our definition.

This approach to equilibrium topology naturally gives rise to properties that are robust to perturbations including spatial disorder and weak interactions [41,42]. In addition, such a definition (which is in terms of the bulk) correctly predicts the existence of gapless boundary edge modes. We show in this section that one can take a similar approach to classifying the topology of nonequilibrium states in a way that inherits all these important properties. These arguments apply to both noninteracting and interacting systems.

Although equilibrium topology is commonly associated with physical observables, such as the Hall conductance, which manifestly depend on the full Hamiltonian, topological phases can be identified solely from the many-body ground state. This is evident for noninteracting fermions: Starting with a single-particle Hamiltonian $\hat{\mathcal{H}} = \hat{\psi}_i^\dagger \mathsf{H}_{ij} \hat{\psi}_j$ with single-particle energies E_λ, one can perform the spectral flattening procedure [15,16,43], where one smoothly modulates all the energies E_λ to $\operatorname{sgn} E_\lambda = \pm 1$ without changing the eigenstates. Since this is a continuous deformation of the system which can be done without breaking any symmetry or closing the gap, the resultant Hamiltonian is topologically identified with the physical one. We arrive at the flat-band Hamiltonian Q which is related to the single-particle density matrix $\rho_{ij} = \langle \Psi_0 | \hat{\psi}_i^\dagger \hat{\psi}_j | \Psi_0 \rangle$ by $\mathsf{Q} = 1 - 2\rho$. This matrix ρ is determined by the ground state of $\hat{\mathcal{H}}$ only. We see that all equilibrium topological properties are uniquely determined by two objects: (1) a single many-body state (the ground state) and (2) a collection of symmetries which define the allowed deformations of that state.

The above formulation of equilibrium topology has a natural nonequilibrium generalization: We can use the time evolved state $|\Psi(t_\mathrm{f})\rangle$ in place of the ground state and use only the symmetries which are generically preserved under time evolution to define the allowed deformations. This is equivalent to constructing some fictitious Hamiltonian $\hat{\mathcal{Q}}(t_\mathrm{f})$ for which $|\Psi(t_\mathrm{f})\rangle$ is the ground state and applying the equilibrium classification. The result is a topological classification which naturally inherits all the attractive physical features of the equilibrium classification.

We will make use of the construction involving the fictitious Hamiltonian $\hat{\mathcal{Q}}(t_\mathrm{f})$ in much of this paper. For concreteness (inspired by the spectral flattening procedure), we can use

$$\hat{\mathcal{Q}}(t_\mathrm{f}) = 1 - |\Psi(t_\mathrm{f})\rangle\langle\Psi(t_\mathrm{f})|. \tag{1}$$

This construction can be applied to any gapped system and at any finite time yields a Hamiltonian with couplings that decay exponentially with spatial separation [44].

Our definition of topology out of equilibrium is rather natural in that it pertains only to properties of $|\Psi(t_\mathrm{f})\rangle$ [or equivalently $\hat{\mathcal{Q}}(t_\mathrm{f})$] and the set of symmetries which the state generically possesses. We expect that our classification scheme will correctly predict all characteristic signatures of topology which are familiar from the study of systems at equilibrium. In particular, nonequilibrium states which are topologically nontrivial under our definition will exhibit a bulk-boundary correspondence, which can be seen through gapless edge modes of the entanglement spectrum [45]. We show this explicitly in Sec. V.

With a less careful definition of nonequilibrium topology, one might expect that any two states that are initialized in topologically distinct wave functions must remain distinct for all time, since one can always evolve backwards in time using $\mathsf{U}(t)^\dagger$ and see that the two states began with different topologies. Such an approach was adopted in previous studies, such as Refs. [33,46]. However, unlike our definition, this interpretation is a characterization of the full historical trajectory of the wave function, since one cannot necessarily make the same conclusions from $|\Psi(t_\mathrm{f})\rangle$ alone. We shall see that this definition would incorrectly predict the dynamics of the entanglement spectrum.

Although the nonequilibrium classification we propose is set up in an analogous way to equilibrium, it can in general differ from the equilibrium classification due to the fact that not all symmetries are generically preserved under time evolution (see Sec. II). This means that the set of allowed deformations of the state in question is wider. Indeed, in equilibrium, two states are topologically equivalent if they can be smoothly deformed between one another without breaking the symmetries in question. However, out of equilibrium, we say that states are equivalent if they can be connected via unitary time evolution under some local Hamiltonian that respects the given symmetries. The former is a stronger statement than the latter.

Furthermore, a naïve expectation may be that the nonequilibrium classification will simply be given by the equilibrium classification under the subset of symmetries which are preserved dynamically. However, this neglects the fact that the initial state itself has some symmetry constraints, which may restrict which topological phases are accessible in the first place. As a simple example in the context of free-fermion systems (which are discussed in Sec. IV), class AII systems in two spatial dimensions featuring time-reversal symmetry are reduced to having no symmetry (class A) once out of equilibrium. Although the equilibrium classification for this reduced symmetry class is the $\mathbb{Z}$-valued Chern number, the nonequilibrium classification will be trivial, since the requirement of a time-reversal invariant initial state necessitates the Chern number to start at zero, which is then preserved throughout evolution.

We schematically illustrate various ways in which the classification can change out of equilibrium in Fig. 1. The four panels (a)–(d) represent possible outcomes for a given set of Hamiltonian symmetries (which we call 'pre-quench symmetries'). After time evolution, the wave function respects only the 'post-quench symmetries,' which are the subset of pre-quench symmetries that are unitary. The possibilities we show are:

(a) The equilibrium classification under the pre-quench and post-quench symmetries is the same, and topologically distinct initial states (ρ_1 and ρ_2) remain topologically distinct for $t > 0$. In this case, ρ_1 will not be able to evolve into a state

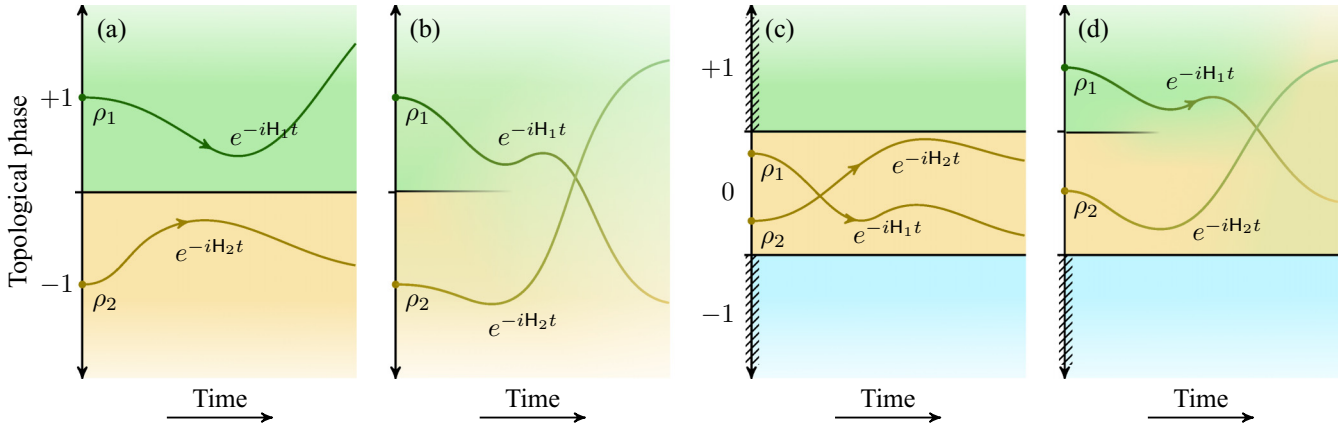

FIG. 1. Illustration of topological restrictions on unitary dynamics. The various topological phases are denoted '0,' '+1,' and '−1.' In each case (a)–(d), some phases are compatible with the symmetry constraints on the initial state, and others are not; the inaccessible phases are marked with hatches. Diagrams (a), (b), and (d) feature initial states ρ_1 and ρ_2 that are separated by an equilibrium topological phase transition (horizontal line), while in (c) the initial states are forced to be in the same equilibrium phase by the initial symmetries. In diagrams (a) and (c), the phase boundaries persist even after dynamically induced symmetry breaking—it is not possible for a state with one topology to evolve into a state with different topology. In (b) and (d), the topological distinction between the two phases is broken out of equilibrium, i.e., the initial state topology is lost under dynamics. In cases (b)–(d), the nonequilibrium classification is trivial due to initial state restrictions and/or the breakdown of equilibrium phase boundaries due to symmetry breaking.

with a different topology, and the 'phase space' that can be explored under unitary dynamics is restricted, as illustrated in Fig. 1(a) (e.g., Class CII in $d = 4$).

(b) The equilibrium classification under post-quench symmetries is trivial. The topologically distinct initial states ρ_1 and ρ_2 become indistinct out of equilibrium, owing to some dynamically-induced symmetry breaking. Once the symmetry is broken for $t > 0$, the topological obstruction between the states is lifted, and there is no restriction on the accessible phase space, as illustrated in Fig. 1(b) (e.g., Class AII in $d = 3$).

(c) The equilibrium classification under post-quench symmetries is nontrivial, but the initial state classification is trivial. The additional symmetry restrictions on initial states ensures that all post-quench states are topologically equivalent, as illustrated in Fig. 1(c) (e.g., Class AI in $d = 2$).

(d) The equilibrium classifications under pre- and post-quench symmetries are both nontrivial, but topologically distinct initial states are indistinct under the post-quench classification, as illustrated in Fig. 1(d) (e.g., Class DIII in $d = 1$, or Class AII in $d = 2$).

It is worth noting that here we are considering systems in the thermodynamic limit or timescales which are subextensive in system size. For finite-sized systems, there will be a time on the order of $t \sim L/v_{\mathrm{L.R.}}$ (where $v_{\mathrm{L.R.}}$ is the Lieb-Robinson velocity) beyond which the correlations of $|\Psi(t)\rangle$ span the system size. At this point the system relaxes back into equilibrium at finite energy density, and our nonequilibrium classification no longer applies. Indeed such a thermalized state does not have a well-defined topology, since the fictitious Hamiltonian $\hat{\mathcal{Q}}(t_{\mathrm{f}})$ will not be local. However, for times less than this thermalization time, the wave-function topology is well defined in the above sense. Additionally, if the system is many-body localized then topology remains well defined for a time which grows exponentially with the system size. In the following section, we apply the formalism described above to systems of noninteracting fermions with nonspatial symmetries, yielding a topological classification that applies to nonequilibrium states.

IV. CLASSIFICATION OF TOPOLOGICAL INSULATORS OUT OF EQUILIBRIUM

The 'tenfold way' of topological insulators [3,14–16] enumerates all topologically distinct phases of noninteracting fermionic systems subject to certain nonspatial symmetry constraints. Specifically, systems in a given spatial dimension d belong to one of ten symmetry classes, depending on the presence of time-reversal (TRS), particle-hole (PHS), and chiral (or sublattice) symmetry [15,47]. Each symmetry is represented by an on-site unitary matrix (T, C, or S, respectively) subject to the constraints $\mathsf{TT}^* = \pm 1$, $\mathsf{CC}^* = \pm 1$ and $\mathsf{S}^2 = +1$ [9]. The entries of the tenfold way are discrete groups (0, $\mathbb{Z}_2$ $\mathbb{Z}$, or $2\mathbb{Z}$), the elements of which represent different topological phases. The structure of the table is shown in Table I for reference. We shall construct a variant of this table which identifies the topological classes that are retained in the post-quench state, assuming that the initial and final Hamiltonians are in the same symmetry class. This is the aim of this section, the results of which are summarized in Table II. Note that one could obtain analogous constructions for which the symmetry classes of the initial state and final Hamiltonians differ, however we do not do so here.

As described in Sec. II, the symmetry properties of the time-evolved state can differ from the symmetry class of the initial state and final Hamiltonian. Of the three symmetries featured in the tenfold way, only PHS is unitary and thus due to dynamically induced symmetry breaking, only PHS is preserved [24]. The post-quench symmetry class is thus either no symmetries (class A), PHS with $\mathsf{CC}^* = +1$ (class D), or $\mathsf{CC}^* = -1$ (class C). As we described in the previous section,

TABLE I. Periodic table of topological insulators at equilibrium [3,14–16]. The ten symmetry classes (two complex and eight real) are listed and given a label s. The zero-dimensional classification is given, from which any dimensional classification can be inferred. For a given dimension d, the equilibrium classification is given by $K_{\mathbb{C}}(s-d \mod 2, 0)$ in the complex classes and $K_{\mathbb{R}}(s-d \mod 8, 0)$ in the real classes.

		Symmetries				Classification
Class		T	C	S	Label s	$K_{\mathbb{C},\mathbb{R}}(s, d=0)$
Complex	A	0	0	0	0	$\mathbb{Z}$
	AIII	0	0	1	1	0
Real	AI	+	0	0	0	$\mathbb{Z}$
	BDI	+	+	1	1	$\mathbb{Z}_2$
	D	0	+	0	2	$\mathbb{Z}_2$
	DIII	−	+	1	3	0
	AII	−	0	0	4	$2\mathbb{Z}$
	CII	−	−	1	5	0
	C	0	−	0	6	0
	CI	+	−	1	7	0

the reduction of symmetry in the post-quench state can lead to a change of topology out of equilibrium.

To construct our classification, we will adopt similar approaches to those used to construct the equilibrium periodic table. In particular, the equilibrium classification can be obtained using the process of *dimensional reduction* [14], in which the physical system is interpreted as a higher dimensional system with one (or more) of its dimensions compactified. This allows the topological properties of lower dimensional systems to be associated with 'parent' systems in higher dimensions. Before generalizing to nonequilibrium states, we first review this procedure for systems in equilibrium, making reference only to properties of the ground state rather than the Hamiltonian.

For simplicity of presentation, we describe strictly noninteracting translationally invariant systems. However, since we are concerned with strong topological invariants, we expect the results to hold in the presence of spatial disorder and weak interactions in a manner analogous to topological systems in equilibrium [41,42]. Such arguments can be applied thanks to the interpretation of $|\Psi(t_f)\rangle$ as the ground state of some local gapped Hamiltonian [Eq. (1)] with nontrivial topology.

A. Dimensional reduction in equilibrium

1. Nonchiral classes

In the absence of symmetry (class A), systems in even dimensions $d = 2n$ can be characterized by the nth Chern number Ch_n. In terms of the Bloch wave functions $|u^\alpha(\vec{k})\rangle$ (where α labels the occupied bands), we define the non-Abelian Berry connection as a 1-form $\mathcal{A}^{\alpha\beta} = \langle u^\alpha(\vec{k})|du^\beta(\vec{k})\rangle$, and the corresponding Berry curvature $\mathcal{F}^{\alpha\beta} = (d\mathcal{A} + \mathcal{A}\wedge\mathcal{A})^{\alpha\beta}$. Then the Chern numbers are given by an integral of the Chern form ch_n over the Brillouin Zone (BZ) [16]

$$\mathrm{Ch}_n = \int_{\mathrm{BZ}} \mathrm{ch}_n\,, \quad \text{where } \mathrm{ch}_n := \frac{1}{(n+1)!}\,\mathrm{Tr}\left(\frac{i\mathcal{F}}{2\pi}\right)^{(n+1)}. \tag{2}$$

Now consider adding either TRS (with $\mathsf{TT}^* = \pm 1$) or PHS (with $\mathsf{CC}^* = \pm 1$), yielding one of the nonchiral classes AI, AII, D, or C. Depending on the dimension and type of symmetry, this may or may not restrict the allowed values of Ch_n. If the Chern number is not restricted by the additional symmetry, then this entry in the periodic table is termed the 'even primary series,' and is $\mathbb{Z}$ classified [16].

Each member of the even primary series induces two $\mathbb{Z}_2$ entries in two lower dimensions, termed the first and second

TABLE II. Classification of topological insulators out of equilibrium. The nonequilibrium classification describes the set of topological classes which remain distinct after time evolution under a Hamiltonian possessing the set of symmetries in question, as outlined in Sec. III. The ten symmetry classes of the tenfold way are listed on the left and defined by the presence (+, −, 1) or absence (0) of time-reversal (T), particle-hole (C), and chiral (S) symmetries [15,47]. For each symmetry class and spatial dimension d, the equilibrium and nonequilibrium classifications are given. A single entry indicates that the classification does not change out of equilibrium, while the notation $G_1 \to G_2$ indicates that the classification changes from G_1 in equilibrium to G_2 out of equilibrium. The different series of the classification are colored as described in the main text, and the references to the discussions of each series are given below the table. Systems in dimension $d > 7$ have the same classification as the corresponding system in $(d-8)$ dimensions (Bott periodicity).

	Symmetries			Spatial dimension d							
Class	T	C	S	0	1	2	3	4	5	6	7
A	0	0	0	$\mathbb{Z}$	0	$\mathbb{Z}$	0	$\mathbb{Z}$	0	$\mathbb{Z}$	0
AIII	0	0	1	0	$\mathbb{Z} \to 0$	0	$\mathbb{Z} \to 0$	0	$\mathbb{Z} \to 0$	0	$\mathbb{Z} \to 0$
AI	+	0	0	$\mathbb{Z}$	0	0	0	$2\mathbb{Z}$	0	$\mathbb{Z}_2 \to 0$	$\mathbb{Z}_2 \to 0$
BDI	+	+	1	$\mathbb{Z}_2$	$\mathbb{Z} \to \mathbb{Z}_2$	0	0	0	$2\mathbb{Z} \to 0$	0	$\mathbb{Z}_2 \to 0$
D	0	+	0	$\mathbb{Z}_2$	$\mathbb{Z}_2$	$\mathbb{Z}$	0	0	0	$2\mathbb{Z}$	0
DIII	−	+	1	0	$\mathbb{Z}_2 \to 0$	$\mathbb{Z}_2 \to 0$	$\mathbb{Z} \to 0$	0	0	0	$2\mathbb{Z} \to 0$
AII	−	0	0	$2\mathbb{Z}$	0	$\mathbb{Z}_2 \to 0$	$\mathbb{Z}_2 \to 0$	$\mathbb{Z}$	0	0	0
CII	−	−	1	0	$2\mathbb{Z} \to 0$	0	$\mathbb{Z}_2 \to 0$	$\mathbb{Z}_2$	$\mathbb{Z} \to \mathbb{Z}_2$	0	0
C	0	−	0	0	0	$2\mathbb{Z}$	0	$\mathbb{Z}_2$	$\mathbb{Z}_2$	$\mathbb{Z}$	0
CI	+	−	1	0	0	0	$2\mathbb{Z} \to 0$	0	$\mathbb{Z}_2 \to 0$	$\mathbb{Z}_2 \to 0$	$\mathbb{Z} \to 0$

Even primary (IV B 1); Even descendants (IV B 2); Odd primary (IV B 3); Odd descendants (IV B 4); $2\mathbb{Z}$ series (IV B 5).

descendants [14]. For concreteness, we study the canonical example of the 4D primary insulator with TRS $\mathsf{T}\mathsf{T}^* = -1$, but all descendants can be understood in analogous ways.

Consider a 3D TRS state characterized by the density matrix $\rho^{(\mathrm{A})}(\vec{k})$ as our physical system. A one-parameter family of states $\rho(\vec{k},\theta)$ can be constructed which connects this insulator at $\theta = 0$ to some trivial TRS insulator ρ^{ref} (which is independent of $\vec{k}$) at $\theta = \pi$. The intermediate 3D states for $0 < \theta < \pi$ need not possess TRS. Now consider closing this path into a loop $\theta = -\pi \to 0 \to \pi \equiv -\pi$ by invoking a 'super-TRS' condition

$$\rho(-\vec{k},-\theta) = \mathsf{T}\rho(\vec{k},\theta)\mathsf{T}^\dagger \quad 0 \leqslant \theta \leqslant \pi. \tag{3}$$

Since $\rho^{(\mathrm{A})}(\vec{k})$ and ρ^{ref} respect TRS, this loop can be made without any discontinuities.

By reinterpreting θ as an extra momentum variable in 4D, $\rho(\vec{k},\theta)$ represents a four-dimensional TRS insulator, which is characterized by the second Chern number Ch_2. Because the reference Hamiltonian ρ^{ref} is $\vec{k}$ independent, we can contract the subregions $\theta = \pm\pi$ to a single point, and so the higher dimensional momentum space is a 'suspension' $\Sigma(\mathrm{BZ})$, as illustrated in Fig. 2.

Following Teo and Kane [48], one can show that the super-TRS condition (3) forces the contributions to Ch_2 for $\theta > 0$ and $\theta < 0$ to be equal, and so we need only consider one hemisphere, which we call $\Sigma^N(\mathrm{BZ})$. The Chern form ch_2 can be written as a total derivative of a 3-form called the Chern-Simons form $\mathrm{ch}_2 = dQ_3$ [16], and so the integral over $\theta > 0$ can be computed as a surface integral on the boundary $\theta = 0$, i.e., the physical BZ. We then have

$$\mathrm{Ch}_2 = 2\int_{\Sigma^N(\mathrm{BZ})} \mathrm{ch}_2 = 2\int_{\mathrm{BZ}} Q_3 =: 2\mathrm{CS}_3, \tag{4}$$

where CS_3 is the Chern-Simons (CS) invariant, which is entirely determined by the physical system at $\theta = 0$.

The CS invariant is gauge invariant only up to an integer. This gauge dependence reflects the fact that different

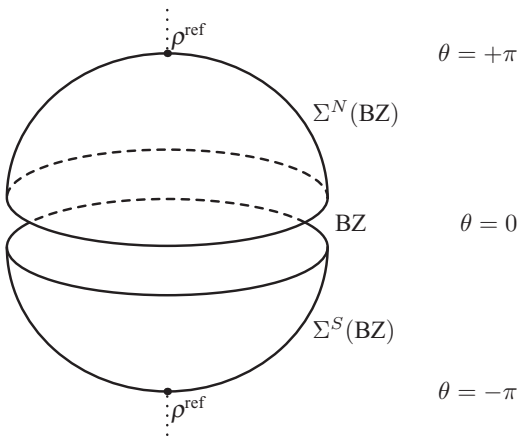

FIG. 2. The physical Brillouin zone (BZ) as the equator of a higher dimensional momentum space $\Sigma(\mathrm{BZ})$ parametrized by $(\vec{k},\theta)$. At the poles $\theta = \pm\pi$, the BZ is contracted to a point, representing the $\vec{k}$-independent reference state. We also identify the two poles, ensuring periodicity in θ.

embeddings of $\rho^{(\mathrm{A})}(\vec{k})$ in 4D can yield Chern numbers that differ by an even integer. $\mathrm{Ch}_2 \mod 2$ defines a $\mathbb{Z}_2$-valued topological invariant which can characterize the 3D system unambiguously—this relates the first descendant (3D) to the primary series (4D) in class AII. A similar construction is also possible for the second descendants, which are classified by the Fu-Kane (FK) invariant [49]

$$\mathrm{FK}_{d=2n} = \int_{\mathrm{BZ}^{1/2}} \mathrm{ch}_n - \int_{\partial\mathrm{BZ}^{1/2}} Q_{2n-1}, \tag{5}$$

where $\mathrm{BZ}^{1/2}$ is the half of the BZ where one of the momenta $0 \leqslant k_i < \pi$, and $\partial\mathrm{BZ}^{1/2}$ is its boundary. To avoid ambiguity, this quantity must be calculated in a particular gauge that is specified by the TRS (or PHS) symmetry operator.

2. Chiral classes

Systems with only chiral symmetry (class AIII) in odd dimensions also inherit their topology from a higher dimensional insulator in a similar way. The procedure is slightly different from the above, in that the higher dimensional insulator has a different symmetry to the physical state. Given a state $\rho^{(\mathrm{A})}(\vec{k})$ which respects a chiral symmetry operator S, we can uniquely specify a higher-dimensional state via [50]

$$\rho(\vec{k},\theta) = \rho^{(\mathrm{A})}(\vec{k})\cos(\theta/2) - \tfrac{1}{2}\mathsf{S}\sin(\theta/2) + \tfrac{1}{2}[1-\cos(\theta/2)]$$
$$\theta \in [-\pi,\pi), \tag{6}$$

where the last term enforces the correct trace. The addition of a term proportional to S breaks the chiral symmetry, and so the $(d+1)$-dimensional Hamiltonian belongs to class A and is characterizable by a Chern number. It can be shown [50] that topologically distinct chiral systems remain topologically distinct in the higher dimension, and vice versa, i.e., this mapping is a bijection between topological classes in different dimensions. Thus chiral systems in odd dimensions are $\mathbb{Z}$ classified according to the Chern number of $\rho(\vec{k},\theta)$. This can be more easily calculated as a winding number ν_{2n+1}, or from the CS invariant calculated in a particular gauge [16].

If TRS or PHS are also present in the physical system (classes BDI, DIII, CII, and CI), then we can still use the mapping (6). In this case the symmetry of the higher dimensional system changes according to [from d to $(d+1)$ dimensions] [16]

$$\mathrm{AIII} \to \mathrm{A}; \quad \mathrm{BDI} \to \mathrm{D}; \quad \mathrm{CII} \to \mathrm{C};$$
$$\mathrm{DIII} \to \mathrm{AII}; \quad \mathrm{CI} \to \mathrm{AI}. \tag{7}$$

These relations are related to the ordering of the symmetry classes given in Tables I and II. If the higher dimensional system belongs to the even primary series, then any Chern number is realizable and we say that the chiral system belongs to the odd primary series, which is also $\mathbb{Z}$ classified.

As in the nonchiral classes, the primary series gives rise to two descendants in the same symmetry class. As in Sec. IV A 1, a super-TRS condition is applied to the higher dimensional insulator, as well as chiral symmetry. In this case the fractional part of the CS invariant ($\mathrm{CS}_{2n+1} \mod 1$) of the higher dimensional system determines the $\mathbb{Z}_2$ index for the physical system.

B. Dimensional reduction out of equilibrium

The above dimensional reduction procedure in equilibrium will motivate our approach to classifying nonequilibrium states. We generalize the method in the following way. Starting with an initial state $\rho(\vec{k}, t = 0)$ belonging to a particular symmetry class in d dimensions, we construct the higher-dimensional insulator in $(d + r)$ dimensions $\rho(\vec{k}, \vec{\theta}, t = 0)$ in the appropriate manner for the equilibrium classification. The physical (d-dimensional) system evolves under a final Hamiltonian $\mathsf{H}^{\mathrm{f}}_{(d)}(\vec{k}, t)$. We then dimensionally extend this final Hamiltonian to $\mathsf{H}^{\mathrm{f}}_{(d+r)}(\vec{k}, \vec{\theta}, t)$ and consider the time evolution of the higher-dimensional system, while ensuring that the $\vec{\theta} = \vec{0}$ subspace remains true to the physical system.

Of course, as in equilibrium, our conclusions regarding the topology of the physical system should be independent of the choice of embedding in this higher dimensional space; however one should be restricted to embeddings which respect the relevant symmetries of the system, e.g., by enforcing the super-TRS condition (3). Furthermore, we are interested in those properties of the system that can be inferred from the instantaneous wave function $|\Psi(t_{\mathrm{f}})\rangle$ alone, without reference to the history of the wave function at previous times $t < t_{\mathrm{f}}$, as in Ref. [24]. If two choices of $\mathsf{H}^{\mathrm{f}}_{(d)}(\vec{k}, t)$ yield the same final state $|\Psi(t_{\mathrm{f}})\rangle$, then our conclusions must be the same for both quench protocols. Crucially, when looking at $|\Psi(t_{\mathrm{f}})\rangle$, one cannot distinguish whether TRS and chiral symmetries are broken dynamically or explicitly, since either process could yield the same final state. We therefore make no assumptions about the symmetry of $\mathsf{H}^{\mathrm{f}}_{(d)}(\vec{k}, t)$ except for the presence/absence of PHS, which can be inferred from $|\Psi(t_{\mathrm{f}})\rangle$.

We note that, although in equilibrium the dimensional reduction parameter θ is often interpreted as a time coordinate which traces out an adiabatic evolution of the ground state, one should not confuse this parameter with the physical (generally nonadiabatic) time evolution in our nonequilibrium protocol. Instead, θ can be thought of as a coordinate which labels a one-parameter family of independent quench protocols.

Having described the general procedure, we now systematically construct our nonequilibrium table of topological insulators, considering each series in turn.

1. Primary series in $d = 2n$

As previously discussed, the primary series in even dimensions refers to the $\mathbb{Z}$-valued entries of the equilibrium table, and these systems are classified by the Chern number. Each member of the even primary series possesses one symmetry (TRS in $d = 4n$ or PHS in $d = 4n + 2$) which, heuristically, is irrelevant for the topology of the system, since the classification is neither restricted nor enriched by its addition. Indeed the Chern number must remain invariant under *any* smooth gap-preserving deformations of the wave function, even if the underlying symmetries are broken.

Under unitary dynamics, the topology of the state is captured by the fictitious Hamiltonian $\hat{\mathcal{Q}}(t_{\mathrm{f}})$ defined in (1). The time t parametrizes a smooth deformation connecting $\hat{\mathcal{Q}}(0)$ to $\hat{\mathcal{Q}}(t_{\mathrm{f}})$, and therefore the Chern number (and hence the topology) of the initial state must be preserved in time. This behavior has been proved for two dimensions in previous studies [18–21,51]. Note that for finite systems, beyond a certain time $t \sim L/v_{\mathrm{L.R.}}$ the correlations of $|\Psi(t)\rangle$ will span the whole system, at which point the Chern number is no longer a well-defined quantity. The primary series in $d = 2n$ are colored black in Table II.

2. First and second descendants in $d = 2n - 1$ and $d = 2n - 2$

The first and second descendants of the even primary series are constructed as described in Sec. IV A 1. Consider now the dynamics of the higher dimensional insulator.

If the descendants are PHS-protected (class D in $d = 0, 1$ and class C in $d = 4, 5$), then we can impose particle-hole symmetry on the dimensionally extended initial state $\rho(\vec{k}, \vec{\theta}, t = 0)$ and final Hamiltonian $\mathsf{H}^{\mathrm{f}}_{(d+r)}(\vec{k}, \vec{\theta}, t)$. This ensures that the PHS of the higher dimensional system is preserved in time, and so $\rho(\vec{k}, \vec{\theta}, t)$ will also respect PHS; the connection between insulators of different dimensions thus holds out of equilibrium. Moreover, the descendants inherit their topology from the even primary series, the topology of which is preserved (Sec. IV B 1). Therefore the topology of the descendants will not change in time.

However, if the descendants are TRS-protected (class AII in $d = 2, 3$ and class AI in $d = 6, 7$), then for $t > 0$ the $(d + r)$-dimensional state $\rho(\vec{k}, \vec{\theta}, t)$ will *not* respect TRS due to dynamically induced symmetry breaking. Even though the Chern number of $\rho(\vec{k}, \vec{\theta}, t)$ cannot change in time, the connection between the insulators of different dimension no longer holds. Indeed for first descendants, the relationship (4) between Ch_n and CS_{2n-1} no longer holds, because the contributions to Ch_n for $\theta > 0$ and $\theta < 0$ are not equal once TRS is dynamically broken. Therefore the topology of TRS-protected first descendants is lost out of equilibrium.

For the first TRS descendants, we expect that the CS invariant will be free to vary continuously in time since there is no symmetry to quantize CS_{2n-1} for $t > 0$, in a similar way to class AIII in 1D [24]. This in turn implies that the second descendants, which themselves inherit their topology from the first descendants, must also lose their topology out of equilibrium. Unlike the first descendants, the relevant bulk index for second descendants [the FK invariant Eq. (5)], does not vary in time [46], however the above argument highlights that the relevance of the FK invariant to topology is lost when out of equilibrium. Indeed the FK invariant is only meaningful when a gauge determined by the TRS is adopted; once TRS is dynamically broken this gauge is no longer uniquely specified and thus the topology is lost. All the cases covered in this section are marked in blue in Table II.

3. Primary series in $d = (2n - 1)$

We now turn to $\mathbb{Z}$-classified systems that feature a chiral symmetry, which constitute the odd primary series. In equilibrium, these systems are often analyzed in terms of winding numbers [15] without reference to dimensional reduction. However, once chiral symmetry is broken, the density matrix can no longer be brought into a canonical off-diagonal form and so the usual definition of the winding number is no longer well defined. We will instead make reference to the dimensional reduction procedure outlined in Sec. IV A 2. Let

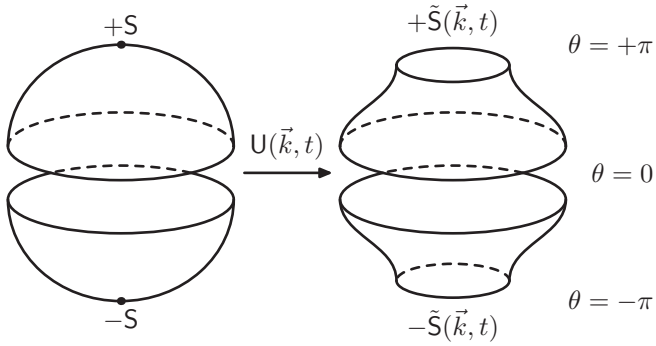

FIG. 3. Dimensional extension of a chiral symmetric insulator after unitary time evolution. The higher dimensional BZ, which was compact at the poles $\theta = \pm\pi$, becomes open for $t > 0$.

us start with the case where no additional symmetries are present (class AIII in $d = 2n - 1$).

In equilibrium, the primary series in $d = (2n - 1)$ can be related to the primary series in $(d + 1)$ dimensions via the extension (6), and so we consider the time evolution of this $(d + 1)$-dimensional insulator. As was highlighted at the beginning of Sec. IV B, we should not be able to distinguish explicit chiral symmetry breaking from dynamically induced symmetry breaking, and so we should not assume that $\mathsf{H}^{\mathrm{f}}_{(d)}(\vec{k}, t)$ is chiral. Therefore we no longer have a unique prescription for dimensionally extending the final Hamiltonian, and so we can choose an arbitrary θ dependence for $\mathsf{H}^{\mathrm{f}}_{(d+1)}(\vec{k}, \theta, t)$.

Here we note an important difference between the dimensional extensions described in Secs. IV A 1 and IV A 2. In the former, the higher-dimensional insulator exhibits periodicity in the θ direction, due to the TRS/PHS of the reference system; this ensures that the BZ remains closed for all times, regardless of the choice of $\mathsf{H}^{\mathrm{f}}_{(d+1)}(\vec{k}, \theta, t)$. However, as can be seen from (6), the parent systems of chiral insulators are not periodic in θ; rather, the closure of the BZ comes from the $\vec{k}$ independence of the state at the poles $\theta = \pm\pi$, which allows the poles to be compactified (see, e.g., Ref. [50]). Since we are free to choose any embedding of $\mathsf{H}^{\mathrm{f}}_{(d+1)}(\vec{k}, \theta, t)$, the $\vec{k}$ independence at the poles may fail. Thus a boundary of the higher dimensional system may open up at $\theta = \pm\pi$, as illustrated in Fig. 3.

Because the BZ is no longer a closed manifold, the integral of the Chern form $\int_{\mathrm{BZ}} \mathrm{ch}_n$ is no longer quantized, as contributions can 'leak' out through the boundary at $\theta = \pm\pi$. We could try to redefine a topological invariant by subtracting off the surface integral at the boundary, yielding a quantized index

$$\mu(t)_{\mathrm{AIII}} := \int_{\mathrm{BZ}_{(d+1)}} \mathrm{ch}_n(t) - \int_{\partial \mathrm{BZ}_{(d+1)}} Q_{2n-1}(t), \qquad (8)$$

where the surface $\partial \mathrm{BZ}_{(d+1)}$ refers to the boundaries at $\theta = \pm\pi$. However, while $\mu(t)_{\mathrm{AIII}}$ is quantized to an integer, its value is gauge dependent since the second term is gauge invariant only up to an integer. Therefore we cannot ascribe any physical meaning to $\mu(t)_{\mathrm{AIII}}$. Clearly, the topology of class AIII systems is lost out of equilibrium.

For members of the primary series that possess TRS and PHS in addition to chiral symmetry, we must also consider the symmetry of the higher-dimensional system, which is given by (7). As before, the presence of TRS in the final Hamiltonian is irrelevant since the symmetry will be dynamically broken. However, if the higher dimensional system possesses PHS (as for BDI and CII), then we should also impose PHS on $\mathsf{H}^{\mathrm{f}}_{(d+1)}(\vec{k}, \theta, t)$, thereby preserving the symmetry of $\rho(\vec{k}, \vec{\theta}, t)$. As we found for the nonchiral classes, these PHS-respecting embeddings ensure that contributions to $\int_{\mathrm{BZ}} \mathrm{ch}_n$ are equal for $\theta < 0$ and $\theta > 0$, so we can only consider the upper half $\theta > 0$. Now we can construct an index analogous to that defined in (8)

$$\mu(t)_{\mathrm{PHS}} := 2 \int_{\theta>0} \mathrm{ch}_n(t) - 2 \int_{\theta=+\pi} Q_{2n-1}(t). \qquad (9)$$

This index is quantized to an integer, and owing to the factor of 2, gauge transforms can only change $\mu(t)_{\mathrm{PHS}}$ by an *even* integer. Thus the parity $\mu(t)_{\mathrm{PHS}} \mod 2$ serves as a topological index which is preserved under unitary dynamics. Evidently, $\mu(t)_{\mathrm{PHS}} \mod 2$ equals the parity of the $(d + 1)$-Chern number at $t = 0$. Additionally, if the first term of (9) is evaluated using Stokes' theorem, then we find $\mu(t)_{\mathrm{PHS}} = 2\mathrm{CS}_{2n-1}(t)$. In essence, primary systems in classes BDI and CII are reduced to first descendants of even-dimensional systems, which have a $\mathbb{Z}_2$ classification. However for classes DIII and CI, the absence of PHS in the higher dimensional system results in the loss of topology for the same reasons as in class AIII. The odd primary series are marked in red in Table II.

4. First and second descendants in $d = (2n - 1) - 1$ and $d = (2n - 1) - 2$

$\mathbb{Z}_2$-classified insulators in the chiral classes inherit their topology from the odd primary series. Clearly, if the parent system loses its topology out of equilibrium (as is the case for classes DIII and CI), then its descendants will also lose their topology.

On the other hand, in classes BDI and CII, the parent insulator is reduced from a $\mathbb{Z}$-classified primary insulator to the $\mathbb{Z}_2$-classified first descendant of the even primary series. We construct a higher-dimensional initial state in the same symmetry class according to Sec. IV A 1 and time evolve under a PHS Hamiltonian. The $\mathbb{Z}_2$ classification of the descendant matches the *parity* of the higher-dimensional winding number. Therefore, despite the reduction of the higher dimensional system from $\mathbb{Z}$ to $\mathbb{Z}_2$, the topology of the physical system is preserved, as it only depends on the bulk index modulo 2. We see that the first descendant of the odd primary series becomes the second descendant of the even primary series.

The second descendants of the odd primary series are $\mathbb{Z}_2$ classified in equilibrium; however generalizing the above construction would require us to reinterpret them as a *third* descendant of the even primary series. As shown in Ref. [14], one cannot construct a third descendant with a nontrivial topological classification. Therefore, these systems lose their topology out of equilibrium. These systems studied in this section are marked in orange in Table II.

5. $2\mathbb{Z}$ classified systems

The only systems which remain to be classified are those which have a $2\mathbb{Z}$ classification in equilibrium; these occur four dimensions below the primary series. In even dimensions, these are classified by the Chern number just as in the primary series, but the extra symmetry enforces the Chern number to be even [16]. We can employ exactly the same reasoning as in Sec. IV B 1 to show that these systems also preserve their topology out of equilibrium, with the caveat that systems must be initialized with an even Chern number.

Similarly, in odd dimensions the $2\mathbb{Z}$ systems are classified in the same way as the primary series, with the understanding that only even topological indices are possible. We use our results from Sec. IV B 3, which show that in classes CI and DIII (in $d = 3$ and 7, respectively) the topology is lost. In classes CII and BDI (in $d = 1$ and 5, respectively), the parity of the winding number is preserved; however since the initial state must have an even winding number, all states become topologically trivial out of equilibrium. The systems covered in the above are colored green in Table II.

C. Structure of the nonequilibrium classification

Having considered all possible topological systems in all spatial dimensions, we arrive at our nonequilibrium classification given in Table II. Some comments on its structure are required.

The fact that PHS is the only symmetry which is preserved under dynamics indicates that the state [or equivalently the fictitious Hamiltonian (1)] will collapse onto one of the symmetry classes A, D, or C. The equilibrium classification of these classes acts as an 'upper bound,' in that the nonequilibrium entry must be a subgroup of the corresponding equilibrium entry A, D, or C. For example, in $d = 3$ and 7, the equilibrium classifications of classes A, D, and C are all 0, hence all nonequilibrium classifications in $d = 3$ and 7 are 0.

The equilibrium table exhibits two forms of periodicity: Firstly, the table is invariant if all spatial dimensions are shifted by $d \to d + 8$. This is naturally also seen in our nonequilibrium table, since all our arguments are invariant under such an eightfold dimensional shift. The equilibrium table is also invariant if the dimension is increased by one and the symmetry classes are all shifted down. More precisely, the equilibrium classification only depends on $s - d \mod 8$ (2), where s is the label of the real (complex) symmetry class given in Table I. This full periodicity is not reflected in the nonequilibrium classification, because of the differences between the three symmetries: Only PHS is preserved out of equilibrium. However, a subset of this periodicity survives. Between symmetry classes s and $s + 4$, all the symmetries are the same, with the exception that the quantities TT^* and CC^* change sign. Their role under dynamics is therefore the same, and so the nonequilibrium classification for (s, d) is the same as for $(s + 4, d + 4)$.

V. BULK-BOUNDARY CORRESPONDENCE AND ENTANGLEMENT SPECTRA

The arguments of Sec. IV are formulated in terms of characterizations of the bulk of a system. This is a natural approach since bulk topological indices can be directly calculated for a single state composed of full Bloch bands. However, topological phases are also characterizable at their boundary, via the presence of certain gapless edge modes. We expect that one could alternatively derive our nonequilibrium classification by considering boundary modes, in a manner similar to the classification of edge theories in Ref. [15]. Of course, a wave function alone does not itself possess edge excitations, since these are properties of a Hamiltonian spectrum, so these edge modes are not directly observable, but through our constructions described in Sec. III, we can associate an edge theory to a state.

Specifically, since the topology of $|\Psi(t_\mathrm{f})\rangle$ is given by the equilibrium topology of some fictitious Hamiltonian [e.g., $\hat{\mathcal{Q}}(t_\mathrm{f})$ in Eq. (1)], we can consider the edge modes of this fictitious Hamiltonian. In the case of noninteracting fermions, we can calculate the time-evolved Bloch functions $|u^\alpha(\vec{k}, t)\rangle = e^{-i\mathsf{H}^\mathrm{f}(\vec{k})t}|u^\alpha(\vec{k}, 0)\rangle$ for an infinite system and then construct a noninteracting translationally invariant Hamiltonian $\mathsf{Q}(\vec{k}, t_\mathrm{f})$ for which $|\Psi(t_\mathrm{f})\rangle$ is the ground state. A real-space Hamiltonian $\mathsf{Q}(t_\mathrm{f})$ can then be constructed from $\mathsf{Q}(\vec{k}, t_\mathrm{f})$ and given a boundary of codimension 1. If $|\Psi(t_\mathrm{f})\rangle$ is topological, then gapless modes will appear at this edge.

This is a rather indirect way of probing the bulk-boundary correspondence associated with the topology of $|\Psi(t_\mathrm{f})\rangle$, in part due to the fact that the choice of $\mathsf{Q}(t_\mathrm{f})$ is not uniquely defined. A simpler strategy is to make use of the entanglement spectrum [45], which is uniquely defined and can be calculated directly from the wave function $|\Psi(t_\mathrm{f})\rangle$. In equilibrium, the entanglement spectrum reflects edge modes of the governing Hamiltonian and can be computed from the ground state alone. By analogy, studying the entanglement spectrum of $|\Psi(t_\mathrm{f})\rangle$ is a simple and direct way to detect the edge modes of $\hat{\mathcal{Q}}(t_\mathrm{f})$. To be specific, we partition the system into regions A and B and consider the reduced density matrix $\hat{\rho}_A = \mathrm{Tr}_B\,|\Psi(t_\mathrm{f})\rangle\langle\Psi(t_\mathrm{f})|$. If the nonequilibrium state is topologically nontrivial, then we should see gapless entanglement modes in the entanglement Hamiltonian $\hat{\mathcal{H}}_E = -\ln\hat{\rho}_A$. Although there may be quantitative differences between the spectrum of $\hat{\mathcal{Q}}(t_\mathrm{f})$ and the entanglement spectrum, the gaplessness of one spectrum implies that the other spectrum is gapless [43].

The entanglement spectrum is more computationally practical, and we will present numerical results for the entanglement spectrum in Sec. V B. However, since the two edge theories described above are equivalent, we simply refer to the fictitious Hamiltonian $\mathsf{Q}(t_\mathrm{f})$ in our analysis, again considering cases where the initial and final Hamiltonians are in the same symmetry class.

A. Edge theory analysis

At $t = 0$, the Hamiltonian $\mathsf{Q}(t = 0)$ will belong to the prequench symmetry class in question and will possess an edge theory associated with the topological phase of H^i. After time evolution, the Hamiltonian $\mathsf{Q}(t_\mathrm{f})$ will belong to a symmetry class (A, D, or C), which may be reduced due to dynamically induced symmetry breaking. Terms which were forbidden by TRS or chiral symmetry at $t = 0$ may then appear in $\mathsf{Q}(t_\mathrm{f})$. If these extra terms are able to gap out the edge modes, then

the boundary theory becomes trivial and topology is lost. However, if the edge modes survive for $t > 0$, then topology is preserved.

In the following, we describe certain cases where edge modes are either preserved or destroyed; this analysis is not exhaustive, but it is clear how to generalize the arguments to arrive at Table II. We neglect cases where the equilibrium classification of class A, D, or C is trivial, since in these cases $\mathsf{Q}(t_f)$ will be unable to support any edge modes, regardless of the initial state.

1. 1D superconducting chains

The edge modes of one-dimensional systems are simply discrete modes at the zero-dimensional edges of the system. We compare classes BDI, D, and DIII, all of which reduce to class D for $t > 0$, and are realizable as topological superconductors [52–54].

The edge states of these superconducting classes are all composed of Majorana fermions. In class D, the nontrivial phase simply hosts one Majorana fermion $\hat{\gamma}^{L(R)}$ at each edge L or R. The addition of extra symmetries allows different types of Majorana to appear. Class BDI systems with a winding number ν will possess $|\nu|$ chiral Majorana zero modes at each end $\hat{\gamma}_1^{L(R)}, \ldots, \hat{\gamma}_{|\nu|}^{L(R)}$, whereas nontrivial DIII systems possess a Kramers pair of Majorana fermions at each end $\hat{\gamma}_{\mathrm{I}}^{L(R)}, \hat{\gamma}_{\mathrm{II}}^{L(R)}$ [50] (here, Roman numerals label the two Kramers-degenerate states). After time evolution, chiral and TRS symmetries are broken, which allows local symmetry-breaking terms to appear in $\mathsf{Q}(t_f)$. Majorana fermions on the same edge will be able to couple in pairs, but as long as PHS is preserved Majoranas on opposite ends cannot couple, and Majoranas cannot couple to the bulk [52]. Any two Majoranas which do couple will become gapped. It is clear that in the DIII case, the existence of two Majoranas at each end means that this Kramers pair will in general become gapped, leading to a trivial edge theory and hence a reduction of topology. On the other hand, in class BDI the $|\nu|$ Majoranas on a given edge will gap out in pairs. If $|\nu|$ is even, then all Majoranas will gap out and the edge theory will be trivial, but if $|\nu|$ is odd then one Majorana on each end will survive, corresponding to a nontrivial class D system. Therefore the $\mathbb{Z}$ classification of BDI is reduced to $\mathbb{Z}_2$, in agreement with Sec. IV.

2. 2D insulators

One can also make a similar analysis of the 1D edge modes of 2D systems. We contrast the chiral edge modes of class A systems with the TRS-protected helical modes of AII insulators [55]. When $\mathrm{Ch}_1 = +1$, the class A edge theory can be described using only one band, while the class AII edge features two bands (representing the spin degree of freedom). Taking a boundary perpendicular to the x direction, the two edge theories can be written as

$$\mathsf{H}_{\mathrm{A}}^{\mathrm{b}}(k_x) = v k_x; \quad \mathsf{H}_{\mathrm{AII}}^{\mathrm{b}}(k_x) = v k_x \sigma^z, \tag{10}$$

where $\sigma^{x,y,z}$ are the Pauli matrices in spin space. The TRS operator in the AII case takes the form $\mathsf{T} = i\sigma^y$. The gapless nature of each edge theory is robust, in the sense that symmetry-respecting perturbations cannot open up a gap. For class A, this is simply due to the lack of other states to scatter into, whereas in class AII the TRS forbids any term that could open up a gap at $k_x = 0$.

After a quench, the class A edge theory will remain gapless for the same reasons as in equilibrium; however for class AII, dynamically induced symmetry breaking allows TRS-breaking terms to appear in the edge theory. For example, the term $m\sigma^x$, which is allowed after time evolution, will gap out the edge theory. Clearly, the $\mathbb{Z}_2$ edge mode is unstable under unitary dynamics, and the nonequilibrium topological classification can be identified as $\mathbb{Z}_2 \to 0$.

B. Numerical results for the entanglement spectrum

We supplement our analytical results on the dynamics of edge modes with some numerical simulations of the entanglement spectrum dynamics for 2D insulators. We use the Haldane model [56] and the Kane-Mele model [55] as hosts of nontrivial class A and AII systems, respectively. We take periodic boundary conditions in the x direction and make the entanglement cut perpendicular to the y direction so that the wave vector k_x is a good quantum number, as illustrated in Fig. 4.

The Haldane model describes spinless fermions $\hat{c}_i^{(\dagger)}$ hopping on a honeycomb lattice (with sublattices A and B), with Hamiltonian

$$\hat{\mathcal{H}}_{\mathrm{Hal}} = J_1 \sum_{\langle j,k\rangle} (\hat{c}_j^\dagger \hat{c}_k + \mathrm{H.c.}) + J_2 \sum_{\langle\langle j,k\rangle\rangle} (e^{i\phi_{jk}} \hat{c}_j^\dagger \hat{c}_k + \mathrm{H.c.}) + m \sum_{j\in A} \hat{c}_j^\dagger \hat{c}_j - m \sum_{j\in B} \hat{c}_j^\dagger \hat{c}_j, \tag{11}$$

where $\langle j,k\rangle$ denotes nearest neighbors, and $\langle\langle j,k\rangle\rangle$ denotes next-nearest neighbors. The phases ϕ_{jk} originate from a staggered magnetic flux and are equal to $+\phi$ for anticlockwise hopping about their common nearest neighbor and $-\phi$ for clockwise hopping. The mass term m serves to break the inversion symmetry of the lattice. The model possesses two bands associated with the sublattice degree of freedom and realizes Chern numbers of 0, $+1$, and -1.

The Kane-Mele model has the same honeycomb structure but features spinful fermions $\hat{c}_{i,\alpha}^{(\dagger)}$ where $\alpha = \uparrow, \downarrow$. Instead of a complex hopping (which breaks TRS), the model features a spin-orbit interaction as well as a Rashba interaction. The Hamiltonian is

$$\hat{\mathcal{H}}_{\mathrm{KM}} = J_1 \sum_{\langle j,k\rangle,\alpha} (\hat{c}_{j,\alpha}^\dagger \hat{c}_{k,\alpha} + \mathrm{H.c.}) + i\eta_{\mathrm{s.o.}} \sum_{\langle\langle j,k\rangle\rangle,\alpha,\beta} \nu_{j,k} \hat{c}_{j,\alpha}^\dagger \sigma_{\alpha,\beta}^z \hat{c}_{k,\beta}$$

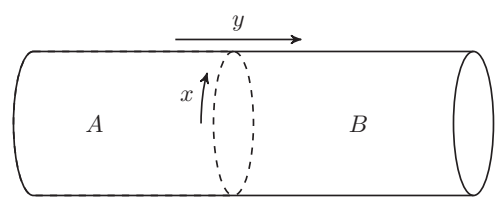

FIG. 4. Geometry of the entanglement cut for 2D systems with periodic boundary conditions in the x direction and open boundary conditions with a large system size in the y direction. The dashed line represents the divide between regions A and B.

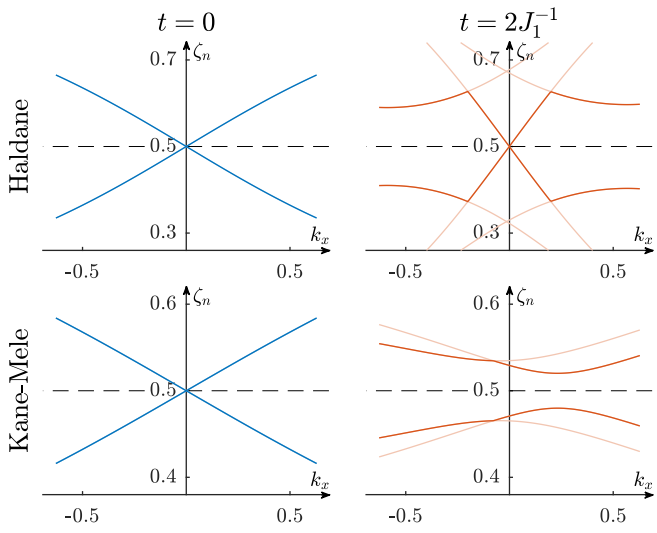

FIG. 5. Dynamics of the single-particle modes of the entanglement spectrum (eigenvalues ζ_n of the reduced single-particle density matrix $C_{i,j} = \langle\Psi(t)|\hat{\psi}_i^\dagger\hat{\psi}_j|\Psi(t)\rangle$, where i, j belong to the spatial region A) for the Haldane model (top) and the Kane-Mele model (bottom). In both systems, we start with a topologically nontrivial initial state at $t = 0$ (left) and then time evolve under a different Hamiltonian by a time $t = 2J_1^{-1}$. The entanglement spectrum of the time-evolved state is plotted (right). In the Haldane model, where topology is preserved, the edge state remains gapless after time evolution. However, in the Kane-Mele model, the gapless modes are TRS protected and topology is destroyed out of equilibrium, hence the edge state becomes gapped at finite times.

$$+ i\lambda_R \sum_{\langle j,k\rangle,\alpha,\beta} \hat{z}\cdot(\vec{\sigma}\times\vec{r}_{j,k})_{\alpha,\beta}\hat{c}^\dagger_{j,\alpha}\hat{c}_{k,\beta}$$
$$+ m\sum_{j\in A,\alpha}\hat{c}^\dagger_{j,\alpha}\hat{c}_{j,\alpha} - m\sum_{j\in B,\alpha}\hat{c}^\dagger_{j,\alpha}\hat{c}_{j,\alpha}, \quad (12)$$

where $\nu_{j,k} = -1$ $(+1)$ for clockwise (anticlockwise) next-nearest neighbor hopping, and $\vec{r}_{j,k}$ is a unit vector in the direction from site j to k. We have also included the inversion symmetry-breaking mass term.

To study the effect of nonequilibrium physics on the entanglement spectra, we construct an initial state as the ground state of the Hamiltonian in question. We then time evolve under a final Hamiltonian which has different parameters and look at the entanglement spectrum of the state after some finite time, which we choose to be $t_f = 2J_1^{-1}$ in both cases. For the Haldane model quench, we choose $(J_1, J_2, \phi, m)_{t=0} = (1, 0.3, 0.4, 0.1)$ and then change the phase to $(\phi)_{t_f} = -0.2$. For the Kane-Mele model quench, we choose $(J_1, \eta_{s.o.}, \lambda_R, m)_{t=0} = (1, 0.5, 0.1, 0.2)$ and then change the spin-orbit coupling to $(\eta_{s.o.})_{t_f} = 1.5$. Using the method of Peschel [57], we obtain the entanglement spectrum by diagonalizing the 'correlation matrix' (or the reduced single-particle density matrix) $\mathsf{C}_{i,j} = \langle\Psi(t)|\hat{\psi}_i^\dagger\hat{\psi}_j|\Psi(t)\rangle$. The eigenvalues of C are related to the single-particle excitation energies ϵ_n of the entanglement Hamiltonian $\hat{\mathcal{H}}_E$ via $\zeta_n = (e^{\epsilon_n}+1)^{-1}$. Therefore an eigenvalue equal to $\zeta = 0.5$ signals an entanglement degeneracy $\epsilon_n = 0$. The results are shown in Fig. 5. We see that the entanglement spectrum of the Haldane model remains gapless after the quench, however in the TRS-protected Kane-Mele model, the entanglement edge mode becomes gapped after the quench. This is consistent with our arguments of the previous section.

VI. PHYSICAL CONSEQUENCES

In the previous sections, we have used a number of different theoretical tools to better understand the topological structures of many-body wave functions out of equilibrium. Here we describe some consequences of our results that are directly relevant in experimental scenarios.

A. Preparation and stability of topological states

In an infinite 2D system, the time independence of the Chern number implies that strictly a nontrivial Chern insulator ground state cannot be realized using unitary dynamics alone [20,21]. Additionally, as mentioned in Sec. III, even in a finite-sized system the Chern number remains constant until correlations span the system size, and the standard definition of the bulk invariant breaks down. Thus to realize a ground state of a topologically nontrivial Hamiltonian in cold atom experiments, one must adiabatically ramp the system across some topological phase transition [58,59]. Since the gap closes and the correlation length diverges at the phase transition, one must proceed slowly enough to avoid Landau-Zener tunneling into an excited state. At the transition point, the gap to excited states is on the order of the level spacing $\sim(\Delta E)/N$, where ΔE is the bandwidth of the Hamiltonian, and N is the number of particles in the system. Thus to ensure the fidelity of adiabatic preparation, one must sweep across the transition over a time which grows extensively with the system size.

Our results generalize this observation to all classes of topological insulators and superconductors. Realizing a topological state which has a nontrivial entry classification in Table II cannot be achieved via unitary dynamics alone unless symmetries are explicitly broken in the governing Hamiltonian or we proceed by slow adiabatic evolution. On the other hand, for systems which have trivial entries in Table II it is possible to time evolve from a trivial state to a topological one over a time which does not grow with the system size while respecting the symmetries of the Hamiltonian. Note that alternative nonadiabatic approaches to preparing topological states have recently been proposed which involve nonunitary dynamics, i.e., interaction between the system and its environment [60,61].

Conversely, topological states which are trivial under our nonequilibrium classification are generically unstable to time-dependent perturbations, for example external noise. In such systems, any fluctuations of the Hamiltonian with frequency component above the bulk gap will generically result in a state which has trivial topology. However, if the topological phase in question is stable out of equilibrium, then even in the presence of these fluctuations, the wave function will possess the same topology which it was initialized with.

Analogously, since in equilibrium bulk topological phases are intimately related with the protection of their edge modes, we expect that this instability of certain phases to time-dependent perturbations will also have important effects for

the robustness of edge modes in general. In the following two sections, we study examples of these instabilities.

B. Local adiabatic mixing of edge modes

One proposed practical use of topological states is in quantum information technology [62,63]. The nonlocal entanglement associated with 0D edge or defect modes allows for robust qubit storage over timescales that grow exponentially with system size—indeed this was the original motivation of Kitaev's proposal to realize Majorana fermions [52]. These edge modes are protected against static perturbations by the bulk topological phase in equilibrium. However, in cases where the bulk topological phase is destroyed out of equilibrium, we expect that the edge modes will not be protected against time-dependent perturbations. Here we discuss the way in which this dynamical instability affects 0D modes at the edges of 1D systems, however we expect that similar instabilities should arise for edge modes in higher dimensions, with equally important experimental consequences.

To facilitate quantum computation using 0D edge modes, one will need to be able to externally manipulate these topological qubits, which could be done through local adiabatic variation of some system parameters. The requirement of adiabaticity ensures that the qubit cannot couple to the bulk states, which are gapped out. However, the presence of Majorana edge modes implies the existence of an (almost) zero-energy subspace, which can be understood using degenerate adiabatic theory. Within this zero-energy subspace, there is no *energetic* protection against transitions between different zero-energy modes when the Hamiltonian is varied in time, regardless of how slowly the variation is done. However, the modes may still be protected against mixing due to the symmetries that protect the bulk topological phase.

From a practical perspective, we should distinguish mixing between Majoranas which is desired and that which is undesired. The desired mixing will generally involve moving the Majoranas on a global scale, so that their nontrivial braiding statistics can be exploited [64,65]. The nonlocality of this process ensures that it cannot happen 'accidentally,' i.e., through a lack of control over the system. Conversely, any process which can happen locally is generally undesired, in that these processes could occur accidentally. Here we focus on the latter class of processes, and as such we will consider only a local part of the adiabatic low-energy subspace. Any mixing between edge modes within this local subspace is thus undesirable for quantum computation.

As the adiabatic process evolves, one must consider the full dynamics of this local low-energy subspace, which we assume is fully isolated from the bulk. Crucially, one should account for the possibility of dynamically induced symmetry breaking within this subspace and the associated reduction of topology described in the previous sections. Two edge modes which were protected against mixing by symmetry in equilibrium may be able to mix when the Hamiltonian is externally varied in time, because the symmetry which protects them is broken dynamically—this indicates that such qubits would be susceptible to undesired local mixing. This local adiabatic mixing has been predicted in the specific case of class DIII in 1D [66], and here we provide a framework by which this phenomenon can be understood more generally.

The question of which topological modes are vulnerable to local adiabatic mixing is exactly equivalent to our previous consideration of which bulk topological phases are destroyed out of equilibrium, since both problems reduce to the question of whether time-reversal and chiral symmetry-breaking terms are enough to lift the equilibrium topological protection. We therefore expect that our classification (Table II) should generalize the results of Ref. [66] to all symmetry classes, in that entries which become trivial out of equilibrium indicate that the edge modes can adiabatically mix due to local perturbations and therefore are inappropriate for qubit storage.

As an example, we consider 1D systems in class BDI which are in phases with winding number $|\nu| > 1$. Such systems would be expected to host $|\nu|$ chiral Majorana modes at an edge; however when nonequilibrium effects are considered, the topological classification reduces from $\nu_{\text{eq.}} \in \mathbb{Z}$ to $\nu_{;\text{eq.}} \in \mathbb{Z}_2$. As a toy model of such a system (analogous to the one used to demonstrate mixing in class DIII in Ref. [66]), we use a semi-infinite extended Kitaev chain with beyond-nearest-neighbor hopping and pairing [39,67]

$$\hat{\mathcal{H}}_{\nu>0} = \frac{E_g}{2} \sum_{j=1}^{\infty} i\hat{\gamma}_j^B \hat{\gamma}_{j+\nu}^A. \tag{13}$$

Here, we define Majorana operators $\hat{\gamma}_j^A = \hat{c}_j + \hat{c}_j^\dagger$ and $\hat{\gamma}_j^B = -i(\hat{c}_j - \hat{c}_j^\dagger)$ in terms of the spinless fermion creation and annihilation operators $\hat{c}_j, \hat{c}_j^\dagger$. The Hamiltonian features equal amplitude hopping and p-wave superconducting pairing. Clearly, the Majorana modes $\hat{\gamma}_1^A \cdots \hat{\gamma}_\nu^A$ are not involved in the Hamiltonian and hence constitute a local set of zero-energy modes. These modes cannot be gapped out as long as the time-reversal symmetry (associated with the realness of the hopping and p-wave pairing) is preserved. Note that this time reversal symmetry ensures that terms with an even number of 'A' or 'B' labels are not allowed, e.g., $\hat{\gamma}_j^A \hat{\gamma}_k^A$ is forbidden.

Class BDI in $d = 1$ has a nonequilibrium classification $\mathbb{Z} \to \mathbb{Z}_2$, and so when $\nu = 2$ we expect the topological protection of edge modes to be lifted. For this value of ν, we only need to consider six Majorana operators: $\hat{\gamma}_{1,2,3,4}^A$ and $\hat{\gamma}_{1,2}^B$, since all other operators decouple. We consider gradually turning on additional terms in the Hamiltonian which satisfy all the required symmetries and act only on these six local Majoranas. Two such terms are

$$\begin{aligned} \hat{\mathcal{H}}_\mu &= \frac{i\mu}{2}\left[\hat{\gamma}_1^A \hat{\gamma}_1^B + \hat{\gamma}_2^A \hat{\gamma}_2^B\right] \\ \hat{\mathcal{H}}_J &= \frac{iJ}{2}\left[\hat{\gamma}_1^A \hat{\gamma}_2^B + \hat{\gamma}_2^A \hat{\gamma}_1^B\right]. \end{aligned} \tag{14}$$

The first applies a chemical potential to the first two sites, while the second enhances the single-particle hopping between the first two sites. Following Ref. [66], we calculate the degree of mixing between the two modes $\hat{\gamma}_1^A, \hat{\gamma}_2^A$ using a non-Abelian Berry connection. Since the variation is slow with respect to E_g, a Majorana zero mode Γ (which squares to 1) must remain an instantaneous zero-energy eigenstate after time evolution, which means we must have $\Gamma(t) = \cos\varphi(t)\hat{\gamma}_{\vec{\eta}(t)}^{\text{I}} + \sin\varphi(t)\hat{\gamma}_{\vec{\eta}(t)}^{\text{II}}$, where the Roman numerals distinguish the two instantaneous zero modes. The dynamics of

the mixing angle $\varphi(t)$ follow

$$\varphi(t) = \varphi(0) + \int_{\eta(0)}^{\eta(t)} d\vec{\eta} \cdot \mathcal{A}(\vec{\eta}), \tag{15}$$

where the Berry connection is

$$\mathcal{A}(\vec{\eta}) = \tfrac{1}{2}\{\hat{\gamma}_{\vec{\eta}}^{\mathrm{I}}, \vec{\nabla}_{\eta}\hat{\gamma}_{\vec{\eta}}^{\mathrm{II}}\} \tag{16}$$

with associated Berry curvature $\Omega_{ij} = \partial_{\eta_i}\mathcal{A}_{\eta_j} - \partial_{\eta_j}\mathcal{A}_{\eta_i}$. For the model considered above, we find a nonzero Berry curvature $\Omega_{\mu J} = -E_g^2(E_g^2 + \mu^2 + J^2)^{-2}$ [68], indicating that in general there will be a nonzero amplitude for one Majorana mode to evolve into the other.

C. Decoherence of Majorana-based qubit storage due to noise

The local adiabatic mixing described above demonstrates how temporal variation of external parameters can lead to mixing between degrees of freedom that are topologically protected in equilibrium. In the context of quantum computation, such external variation is necessary for manipulating and/or accessing the information held in the Majorana qubits. However, even when the qubit is simply stored and not accessed, local fluctuations due to external noise may be present. These fluctuations, although nondeterministic, can still lead to mixing between the local degrees of freedom if the topological phase in question is unstable in the nonequilibrium classification (Table II). When the noise is accounted for and averaged over, this should result in decoherence of the qubit which was initially stored. In this section, we show that this decoherence can even occur when the noise is statistically time-reversal symmetric, so that there is no external bias between forward and backward time directions in the noise correlation functions. Note that, due to the adiabatic nature of the mixing, this decoherence should appear for arbitrarily small noise frequencies—specifically we show later that the decoherence time to scale with the noise frequency Γ as $\tau_{\mathrm{d}} \sim E_{\mathrm{gap}}^2 V^{-2}\Gamma^{-1}$, where V is the amplitude of the noise. This is in stark contrast to decoherence due to mixing of edge and bulk states, mediated by noise with frequency components above the gap [69–71].

To test our hypothesis that the nonequilibrium classification predicts which topological zero modes are unstable to this decoherence, we numerically simulate systems in classes BDI and DIII in $d = 1$ which are subject to external noise and determine the extent to which information stored in the Majorana modes is lost in time. Moreover, since class BDI has an entry $\mathbb{Z}$ (equilibrium) $\to \mathbb{Z}_2$ (nonequilibrium), we wish to compare systems in that class with different parities of the topological index, thus we take the winding number ν to be 1 (stable) and 2 (unstable). The three models we consider, therefore, are

$$\hat{\mathcal{H}}^{\mathrm{DIII}} = \sum_{j,\sigma}\left[\frac{1}{2}\mu_j\hat{c}_{j\sigma}^{\dagger}\hat{c}_{j\sigma} + J_j\hat{c}_{j\sigma}^{\dagger}\hat{c}_{j+1\,\sigma} + \Delta_j\hat{c}_{j\sigma}^{\dagger}\hat{c}_{j+1\,\sigma}^{\dagger}\right] + \sum_j\left[\Delta_j^{(s)}\hat{c}_{j\uparrow}^{\dagger}\hat{c}_{j\downarrow}^{\dagger} + \alpha_j^R(\hat{c}_{j\uparrow}^{\dagger}\hat{c}_{j+1\downarrow} + \hat{c}_{j\downarrow}^{\dagger}\hat{c}_{j+1\uparrow})\right] + \mathrm{H.c.}; \tag{17a}$$

$$\hat{\mathcal{H}}_{\nu=1}^{\mathrm{BDI}} = \sum_{j,\beta}\left[\frac{1}{2}\mu_{j\beta}\hat{c}_{j\beta}^{\dagger}\hat{c}_{j\beta} + J_{j\beta}\hat{c}_{j\beta}^{\dagger}\hat{c}_{j+1\,\beta} + \Delta_{j\beta}\hat{c}_{j\beta}^{\dagger}\hat{c}_{j+1\,\beta}^{\dagger}\right] + \mathrm{H.c.}; \tag{17b}$$

$$\hat{\mathcal{H}}_{\nu=2}^{\mathrm{BDI}} = \sum_{j}\left[\frac{1}{2}\mu_j\hat{c}_j^{\dagger}\hat{c}_j + J_j\hat{c}_j^{\dagger}\hat{c}_{j+1} + \Delta_j\hat{c}_j^{\dagger}\hat{c}_{j+1}^{\dagger} + J_j^{(2)}\hat{c}_j^{\dagger}\hat{c}_{j+2} + \Delta_j^{(2)}\hat{c}_j^{\dagger}\hat{c}_{j+2}^{\dagger}\right] + \mathrm{H.c.} \tag{17c}$$

Model (17a) features fermions $\hat{c}_{j\sigma}$ with a spin-1/2 index σ, model (17b) features fermions $\hat{c}_{j\beta}$ where the label $\beta = 1, 2$ distinguishes two disconnected chains, and Model (17c), which generalizes the fine-tuned Hamiltonian (13) to include generic terms allowed by symmetry, features spinless fermions $\hat{c}_j$. The various terms featured in the models, all of which can vary spatially, are a chemical potential μ_j, a Rashba spin-orbit coupling term α_j^R, a single-particle hopping amplitude J_j, and a p-wave (s-wave) superconducting pairing amplitude Δ ($\Delta^{(s)}$). The p-wave superconducting and hopping amplitudes can couple fermions either one or two sites apart—this difference allows us to access both the $\nu = 1$ and $\nu = 2$ phases in the class BDI cases. Each single-particle Hamiltonian will respect PHS ($\mathsf{CC}^* = +1$) due to the redundancy of the Bogoliubov-de Gennes description [72]. In addition, when the parameters are real, both systems satisfy a TRS. In the spinful system (17a) the TRS is symplectic ($\mathsf{TT}^* = -1$), putting it in class DIII. On the other hand, the latter two models possess a TRS satisfying $\mathsf{TT}^* = +1$ due to the spinless nature of the fermions and hence belong to class BDI.

The chains are duplicated in the model of (17b) so that each of the three systems possesses four Majorana zero modes, which is the minimum number required to store a qubit without violating the fermion parity superselection rule. Therefore, each model possesses two 'left' $\hat{\gamma}_{\mathrm{L}}^{1,2}$ and two 'right' $\hat{\gamma}_{\mathrm{R}}^{1,2}$ Majorana zero modes, which in models (17a) and (17c) are protected against being gapped out by a time-reversal symmetry (equivalently, a chiral symmetry).

In each case, the low energy subspace consists of four states for which the bulk is in its ground state, and the nonlocal Dirac fermions $\hat{a}^{\alpha} = \hat{\gamma}_{\mathrm{L}}^{\alpha} + i\hat{\gamma}_{\mathrm{R}}^{\alpha}$ ($\alpha = 1, 2$) are occupied or unoccupied. The fermion parity sectors cannot mix, and so for concreteness we consider only the parity sector where an odd number of edge modes are occupied ($\hat{\gamma}_{\mathrm{L}}^1\hat{\gamma}_{\mathrm{R}}^1\hat{\gamma}_{\mathrm{L}}^2\hat{\gamma}_{\mathrm{R}}^2 = +1$) so that the basis states for the qubit are the states $|1, 0\rangle$ and $|0, 1\rangle$, where $|n^1, n^2\rangle$ denotes the states with $\langle\hat{f}^{\alpha\,\dagger}\hat{f}^{\alpha}\rangle = n^{\alpha}$. One can use Pauli operators $\hat{\sigma}^z = i\hat{\gamma}_{\mathrm{L}}^1\hat{\gamma}_{\mathrm{R}}^1; \hat{\sigma}^x = i\hat{\gamma}_{\mathrm{L}}^1\hat{\gamma}_{\mathrm{L}}^2$ as a basis of operators on this qubit space.

As would be expected in practice, the noise which we introduce in these systems is local. Since we are interested in the response of the edge modes, we choose noise sources

which act only on the two leftmost and two rightmost sites in each system independently. At each end, we consider two simultaneous noise terms which are mutually uncorrelated but overlap spatially. (The reason for considering two noise sources is discussed below.) For each term, the time dependence of the parameter $\eta(t)$ in question is an independent random signal which is zero at $t = 0$, has mean equal to its initial value, and with a Lorentzian power spectrum, i.e., the noise correlator $C(t) := \langle \eta(t')\eta(t'+t)\rangle_{\text{noise}} - \langle \eta(t')\rangle^2_{\text{noise}}$ has a Fourier transform $\tilde{C}(\omega) \propto (\omega^2 + \Gamma^2)^{-1}$, where the width Γ characterizes the noise frequency. Note that the noise we consider is statistically time-reversal symmetric, in the sense that $C(t) = C(-t)$.

To quantify the loss of information due to dephasing, we use the 'recovery fidelity' developed by the authors of Ref. [73], wherein the robustness of class D Majorana-based memories to global fluctuations was studied. This quantity characterizes the extent to which the initial information stored can be recovered by some optimal recovery process. To calculate the fidelity, the authors consider two initial pure qubit states, labeled by $+, -$ which are opposite on the Bloch sphere, i.e., states such that the density matrix in the Majorana subspace is $\hat{\rho}_\pm = \hat{\rho}_0^{\text{Bulk}} \otimes (\hat{1} \pm \hat{\sigma}^x)/2$, where $\hat{\rho}_0^{\text{Bulk}}$ is the ground state density matrix of the bulk, and the $\hat{\sigma}^x$ acts in the Majorana subspace. These initial states are then evolved for a time t under the same realization of the noise potential, and the states obtained from different realizations are averaged to obtain mixed density matrices $\hat{\rho}_\pm(t)$. Reference [73] showed that the optimal Gaussian recovery process has a fidelity

$$F^{\text{opt}}(t) = \tfrac{2}{3} + \tfrac{1}{6}\|\Gamma_+(t) - \Gamma_-(t)\|_{\text{op}}. \tag{18}$$

Here, $\|\cdot\|_{\text{op}}$ is the operator norm (which returns the largest eigenvalue), and $\Gamma_\pm(t)_{jk} := \text{Tr}[\hat{\rho}_\pm(t)\hat{\gamma}_j\hat{\gamma}_k]$ is the covariance matrix, where j, k label the set of Majorana operators in the system.

We calculate the time dependence of the fidelity for each of the models (17) and plot the results in Fig. 6. All Hamiltonian parameters are site independent, except for the noise terms acting on the two leftmost sites. The initial Hamiltonian parameters chosen are: $(\mu, J, \Delta, \Delta^{(s)}, \alpha^R)^{\text{DIII}} = (0.25, 1, 1, 0.3, 0.2)$ in (17a), $(\mu, J, \Delta)^{\text{BDI}}_{\nu=1} = (0.25, 1, 1)$ in (17b), and $(\mu, J, J^{(2)}\Delta, \Delta^{(2)})^{\text{BDI}}_{\nu=2} = (0.25, 0.2, 1, 0.3, 1)$. These values are chosen such that the systems are all in the desired phases, and have approximately equal decay lengths for the Majorana wave functions. Noise is introduced at each edge through an explicit time dependence of μ_j and $\Delta_j^{(s)}$ in (17a), $\mu_{j\,\beta=1,2}$ and Δ_j in (17b), and μ_j and Δ_j in (17c) (with $j = 1, 2$ on the left edge, and $j = N-1, N$ on the right edge). In $\hat{\mathcal{H}}^{\text{BDI}}_{\nu=1}$, the noise signals on the two disconnected wires are independent and uncorrelated. These noise signals have an amplitude such that the root mean square of the signal $\sqrt{C(t=0)} = 0.1$. We choose the width of the Lorentzian noise spectrum to be small $\Gamma = 0.02$, so as to minimize coupling of the edges and bulk. The length of each chain is $N = 24$, and the density matrices are averaged over 20 noise realizations.

In model (17b), the bulk topology is preserved under the noise, since the topological index is odd and the nonequilibrium classification for class BDI in $d = 1$ is $\mathbb{Z} \to \mathbb{Z}_2$. As such, the memory stored in the associated edge modes is not susceptible to mixing by low-frequency noise, and as expected the recovery fidelity is unaffected by the noise. On the other hand, models (17a) and (17c) lose their topology according to our classification (Table II). In these cases, the recovery fidelity decays until the states which started with opposite qubit values become indistinguishable from one another. There is thus no way of extracting the qubit in these cases where the system topology is destroyed by nonequilibrium effects.

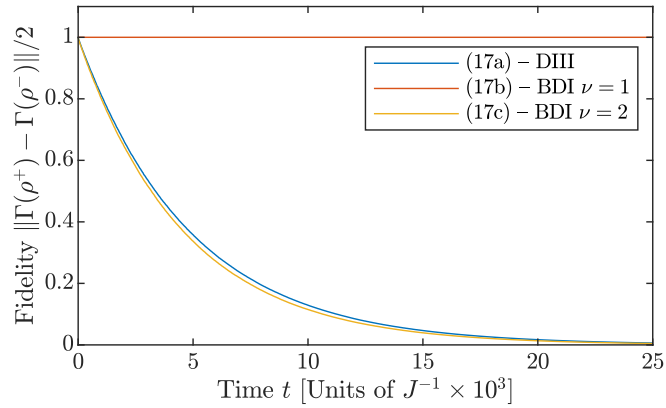

FIG. 6. Decoherence of Majorana qubit memories due to temporal noise, as witnessed by the recovery fidelity [Eq. (18)]. We compare three systems in $d = 1$ [with Hamiltonians given in Eq. (17)], in symmetry classes DIII and BDI—these have entries $\mathbb{Z}_2 \to 0$ and $\mathbb{Z} \to \mathbb{Z}_2$, respectively, in the nonequilibrium classification (Table II). Accordingly, the topology of models (17a) and (17c) is unstable out of equilibrium. This is reflected in the fidelity of storage in the associated Majorana modes when local Lorentzian (TRS) noise is present: The fidelity for the stable model (17b) saturates at a constant value, indicating the preservation of the qubit, whereas the initial state information stored in the unstable models decays away completely, indicating that there is no measurement which can be made to extract the initial qubit state.

Simple arguments can be applied to estimate the rate at which the fidelity decays in Fig. 6. We are generally working in the regime where $E_{\text{maj}} \ll V$, $T^{-1} \ll E_{\text{gap}}$, where E_{maj} is the energy of splitting of the Majoranas (exponentially small in the system size), $V \sim \sqrt{\langle \eta(t)^2 \rangle}$ characterizes the energy scale of the noise term, $T \sim \Gamma^{-1}$ is the time scale over which the signal fluctuates, and E_{gap} is the energy gap of the system. In such a regime, the degenerate adiabatic theorem applies, as described in Sec. VI B (this is independent of the ratio of V and T^{-1}). As such, all mixing effects are purely geometric since any dynamical phases within the low-energy subspace are on the order of E_{maj}. For small V, the dependence of the Berry curvature on the instantaneous value of $\vec{\eta}(t)$ can be neglected [74], so that the angle of mixing between two Majoranas after a time t is $\theta(t) \sim \Omega A(t)$, where $A(t)$ is the signed area swept out by the $\vec{\eta}$ vector over a time t. Clearly, if we only have one noise source, Dim $\vec{\eta} = 1$, then this area is identically zero—this is why we included two (uncorrelated) noise sources in the above. With multiple noise channels, the root mean square area is roughly $\sqrt{\langle A(t)^2 \rangle} \sim V^2(t/T)$. Therefore at short times, the mean-square angle of mixing grows with time as $\sqrt{\langle \theta(t)^2 \rangle} \sim \Omega V^2 t \Gamma$. The Berry curvature

will be on the order of the inverse square of the energy scale of the Hamiltonian $\sim E_{\mathrm{gap}}^{-2}$. Hence the timescale over which the Majoranas mix is $\tau_{\mathrm{d}} \sim E_{\mathrm{gap}}^{2} V^{-2} \Gamma^{-1}$. After averaging over the noise, this leads to a decoherence in the fidelity as $e^{-t/\tau_{\mathrm{d}}}$. Although the above arguments are specific to 0D edge modes, wherein a degenerate adiabatic approximation can be reliably applied, we expect that the relationship between the nonequilibrium destruction of bulk topology listed in Table II and the instability of edge modes against temporal fluctuations should hold generally and in particular be observable in transport signatures.

VII. RELATION TO FLOQUET-SPT PHASES

The nonequilibrium topological classification which we have developed in the previous sections applies rather generally to systems undergoing unitary time evolution in which the time dependence of the Hamiltonian is arbitrary (but symmetry-respecting). There are, however, topological characterizations of nonequilibrium dynamics which apply to more specific protocols, most notably in the dynamics of periodically driven systems, where Floquet-SPT order can emerge [25–28]. It is worth understanding how our results relate to those found in that context.

In order to make connection with observables, we have only considered properties which can be inferred from the wave function $|\Psi(t_{\mathrm{f}})\rangle$ at some instant in time t_{f}. This ensures that the topology which we refer to can be detected using, e.g., the entanglement spectrum. However, if periodicity of dynamics is enforced (either by looking at a Floquet eigenstate, or by considering the steady state of a many-body localized system), then the micromotion over a period can also be characterized. Floquet-SPT order captures the topological properties of this micromotion which cannot be inferred at a single time during the cycle; for that reason, it is fundamentally different from our characterization. Indeed given that generic unitary evolution does not generate periodic evolution of $|\Psi(t)\rangle$, there is no discrete time-translational symmetry in our protocol which is central to the stabilization of Floquet-SPT phases.

This distinction can be seen most clearly in the dynamics of the entanglement spectrum in 1D systems. We have demonstrated that robust nonequilibrium topology of the wave function ensures that entanglement degeneracies are preserved at all times throughout the time evolution. In contrast, as shown in Ref. [27], the pattern of entanglement spectrum dynamics in a Floquet SPT phase is one of 'charge pumping,' where the entanglement energies associated with entanglement eigenstates of opposite symmetry charge are forced to cross each other at some point during the time evolution. Looking at the entanglement spectrum at a particular time in the Floquet system, one would generically observe no degeneracies.

Although the topological characterization of periodic and nonperiodic systems captures different physics, both analyses demonstrate the stark difference between equilibrium and nonequilibrium systems. It is known that Floquet SPT order can emerge independently of the static properties of the Floquet Hamiltonian, which governs the stroboscopic time evolution of one period [29,30]. In the same manner, the wave-function topology which we discuss can be maintained independently of the static properties of the Hamiltonian governing time evolution. Consider as a simple example a quench in which the initial state is the ground state of a TRS-broken insulator with nonzero Chern number, but the final Hamiltonian is time-reversal symmetric. (This quench where the symmetry of the Hamiltonian changes was not covered earlier but can be easily understood in the same manner.) The TRS of the final Hamiltonian implies that its ground state cannot be a Chern-insulating phase, but regardless the wave function $|\Psi(t)\rangle$ will be topologically nontrivial while it evolves under the trivial H^{f}, analogous to the cases studied in Refs. [20,21]. Rather generally, we find that the topological properties of a time-evolving wave function are completely independent from the static topological indices associated with the governing Hamiltonian.

VIII. CONCLUSION

We have developed a formalism by which the topological properties of pure many-body wave functions far from equilibrium can be understood. Importantly, we show that such systems possess a nonequilibrium topological classification which can differ from that in equilibrium. This approach was applied to noninteracting fermionic systems under the 'tenfold way' in arbitrary spatial dimension, which led to our central result, Table II. Robustness to disorder and weak interactions are naturally incorporated in our results, as is familiar from equilibrium topology. The results can be understood using two complementary perspectives: one in terms of bulk properties and one in terms of boundary theories, the latter of which can be probed using the entanglement spectrum. The physical implications of our results were discussed, and we demonstrated that our classification correctly predicts which topological zero-energy modes are unstable to external fluctuating perturbations. This naturally has consequences for the usage of such zero modes as a topological qubit memory.

Recent results on 1D spin chains [24] also indicate that nonequilibrium classifications could be constructed for wider classes of systems that feature strong interactions and/or spatial symmetries. Additionally, understanding further implications of our classification for experimentally relevant settings remains an important challenge. In analogy to our results on decoherence of zero-energy bound states, we expect that the effect of external time-dependent perturbations on bulk and edge mode transport signatures, such as those studied in Ref. [75], will be directly linked with our nonequilibrium classification.

ACKNOWLEDGMENTS

This work was supported by an EPSRC studentship and Grant Nos. EP/K030094/1 and EP/P009565/1, and by an Investigator Award of the Simons Foundation. Statement of compliance with EPSRC policy framework on research data: All data are directly available within the publication.

[1] K. v. Klitzing, G. Dorda, and M. Pepper, New Method for High-Accuracy Determination of the Fine-Structure Constant Based on Quantized Hall Resistance, Phys. Rev. Lett. **45**, 494 (1980).

[2] D. J. Thouless, M. Kohmoto, M. P. Nightingale, and M. den Nijs, Quantized Hall Conductance in a Two-Dimensional Periodic Potential, Phys. Rev. Lett. **49**, 405 (1982).

[3] A. Kitaev, Periodic table for topological insulators and superconductors, AIP Conf. Proc. **1134**, 22 (2009).

[4] J. M. Kosterlitz and D. J. Thouless, Ordering, metastability and phase transitions in two-dimensional systems, J. Phys. C **6**, 1181 (1973).

[5] X. Chen, Z.-C. Gu, and X.-G. Wen, Local unitary transformation, long-range quantum entanglement, wave function renormalization, and topological order, Phys. Rev. B **82**, 155138 (2010).

[6] X.-L. Qi and S.-C. Zhang, Topological insulators and superconductors, Rev. Mod. Phys. **83**, 1057 (2011).

[7] K. Shiozaki and M. Sato, Topology of crystalline insulators and superconductors, Phys. Rev. B **90**, 165114 (2014).

[8] T. Senthil, Symmetry-protected topological phases of quantum matter, Annu. Rev. Condens. Matter Phys. **6**, 299 (2015).

[9] C.-K. Chiu, J. C. Y. Teo, A. P. Schnyder, and S. Ryu, Classification of topological quantum matter with symmetries, Rev. Mod. Phys. **88**, 035005 (2016).

[10] J. Kruthoff, J. de Boer, J. van Wezel, C. L. Kane, and R.-J. Slager, Topological Classification of Crystalline Insulators Through Band Structure Combinatorics, Phys. Rev. X **7**, 041069 (2017).

[11] H. L. Stormer, D. C. Tsui, and A. C. Gossard, The fractional quantum hall effect, Rev. Mod. Phys. **71**, S298 (1999).

[12] M. Z. Hasan and C. L. Kane, Colloquium: Topological insulators, Rev. Mod. Phys. **82**, 3045 (2010).

[13] Y. Ren, Z. Qiao, and Q. Niu, Topological phases in two-dimensional materials: A review, Rep. Prog. Phys. **79**, 066501 (2016).

[14] X.-L. Qi, T. L. Hughes, and S.-C. Zhang, Topological field theory of time-reversal invariant insulators, Phys. Rev. B **78**, 195424 (2008).

[15] A. P. Schnyder, S. Ryu, A. Furusaki, and A. W. W. Ludwig, Classification of topological insulators and superconductors in three spatial dimensions, Phys. Rev. B **78**, 195125 (2008).

[16] S. Ryu, A. P. Schnyder, A. Furusaki, and A. W. W. Ludwig, Topological insulators and superconductors: Tenfold way and dimensional hierarchy, New J. Phys. **12**, 065010 (2010).

[17] N. Fläschner, D. Vogel, M. Tarnowski, B. S. Rem, D. S. Lühmann, M. Heyl, J. C. Budich, L. Mathey, K. Sengstock, and C. Weitenberg, Observation of dynamical vortices after quenches in a system with topology, Nat. Phys. **14**, 265 (2018).

[18] M. S. Foster, M. Dzero, V. Gurarie, and E. A. Yuzbashyan, Quantum quench in a $p + ip$ superfluid: Winding numbers and topological states far from equilibrium, Phys. Rev. B **88**, 104511 (2013).

[19] P. D. Sacramento, Fate of majorana fermions and chern numbers after a quantum quench, Phys. Rev. E **90**, 032138 (2014).

[20] L. D'Alessio and M. Rigol, Dynamical preparation of Floquet Chern insulators, Nat. Commun. **6**, 8336 (2015).

[21] M. D. Caio, N. R. Cooper, and M. J. Bhaseen, Quantum Quenches in Chern Insulators, Phys. Rev. Lett. **115**, 236403 (2015).

[22] J. H. Wilson, J. C. W. Song, and G. Refael, Remnant Geometric Hall Response in a Quantum Quench, Phys. Rev. Lett. **117**, 235302 (2016).

[23] L. Ulčakar, J. Mravlje, A. Ramšak, and T. Rejec, Slow quenches in two-dimensional time-reversal symmetric $\mathbb{z}_2$ topological insulators, Phys. Rev. B **97**, 195127 (2018).

[24] M. McGinley and N. R. Cooper, Topology of One-Dimensional Quantum Systems Out of Equilibrium, Phys. Rev. Lett. **121**, 090401 (2018).

[25] D. V. Else and C. Nayak, Classification of topological phases in periodically driven interacting systems, Phys. Rev. B **93**, 201103 (2016).

[26] C. W. von Keyserlingk and S. L. Sondhi, Phase structure of one-dimensional interacting floquet systems. i. abelian symmetry-protected topological phases, Phys. Rev. B **93**, 245145 (2016).

[27] A. C. Potter, T. Morimoto, and A. Vishwanath, Classification of Interacting Topological Floquet Phases in One Dimension, Phys. Rev. X **6**, 041001 (2016).

[28] R. Roy and F. Harper, Periodic table for floquet topological insulators, Phys. Rev. B **96**, 155118 (2017).

[29] M. S. Rudner, N. H. Lindner, E. Berg, and M. Levin, Anomalous Edge States and the Bulk-Edge Correspondence for Periodically Driven Two-Dimensional Systems, Phys. Rev. X **3**, 031005 (2013).

[30] P. Titum, E. Berg, M. S. Rudner, G. Refael, and N. H. Lindner, Anomalous Floquet-Anderson Insulator As a Nonadiabatic Quantized Charge Pump, Phys. Rev. X **6**, 021013 (2016).

[31] C. Wang, P. Zhang, X. Chen, J. Yu, and H. Zhai, Scheme to Measure the Topological Number of a Chern Insulator from Quench Dynamics, Phys. Rev. Lett. **118**, 185701 (2017).

[32] Z. Gong and M. Ueda, Topological Entanglement-Spectrum Crossing in Quench Dynamics, Phys. Rev. Lett. **121**, 250601 (2018).

[33] C. Yang, L. Li, and S. Chen, Dynamical topological invariant after a quantum quench, Phys. Rev. B **97**, 060304 (2018).

[34] L. Zhang, L. Zhang, S. Niu, and X.-J. Liu, Dynamical classification of topological quantum phases, Sci. Bull. **63**, 1385 (2018).

[35] K. Esaki, M. Sato, K. Hasebe, and M. Kohmoto, Edge states and topological phases in non-hermitian systems, Phys. Rev. B **84**, 205128 (2011).

[36] D. Leykam, K. Y. Bliokh, C. Huang, Y. D. Chong, and F. Nori, Edge Modes, Degeneracies, and Topological Numbers in Non-Hermitian Systems, Phys. Rev. Lett. **118**, 040401 (2017).

[37] H. Shen, B. Zhen, and L. Fu, Topological Band Theory for Non-Hermitian Hamiltonians, Phys. Rev. Lett. **120**, 146402 (2018).

[38] Z. Gong, Y. Ashida, K. Kawabata, K. Takasan, S. Higashikawa, and M. Ueda, Topological Phases of Non-Hermitian Systems, Phys. Rev. X **8**, 031079 (2018).

[39] S. Lieu, D. K. K. Lee, and J. Knolle, Disorder Protected and Induced Local Zero-Modes in Longer-Range Kitaev Chains, Phys. Rev. B **98**, 134507 (2018).

[40] D.-L. Deng, S.-T. Wang, C. Shen, and L.-M. Duan, Hopf insulators and their topologically protected surface states, Phys. Rev. B **88**, 201105 (2013).

[41] Q. Niu and D. J. Thouless, Quantised adiabatic charge transport in the presence of substrate disorder and many-body interaction, J. Phys. A: Math. Gen. **17**, 2453 (1984).

[42] C. Xu and J. E. Moore, Stability of the quantum spin hall effect: Effects of interactions, disorder, and $\mathbb{z}_2$ topology, Phys. Rev. B **73**, 045322 (2006).

[43] L. Fidkowski, Entanglement Spectrum of Topological Insulators and Superconductors, Phys. Rev. Lett. **104**, 130502 (2010).

[44] This follows from the fact that at some finite time the correlations of $|\Psi(t_f)\rangle$, which become the matrix elements of $\hat{\mathcal{Q}}(t_f)$, decay exponentially in space when sufficiently far apart.

[45] H. Li and F. D. M. Haldane, Entanglement Spectrum As a Generalization of Entanglement Entropy: Identification of Topological Order in Non-Abelian Fractional Quantum Hall Effect States, Phys. Rev. Lett. **101**, 010504 (2008).

[46] Z.-G. Liu, L. Xiong, B. Huang, G.-C. Guo, and M. Gong, Topological indexes in symmetry preserving dynamics, arXiv:1802.02931.

[47] A. Altland and M. R. Zirnbauer, Nonstandard symmetry classes in mesoscopic normal-superconducting hybrid structures, Phys. Rev. B **55**, 1142 (1997).

[48] J. C. Y. Teo and C. L. Kane, Majorana Fermions and Non-Abelian Statistics in Three Dimensions, Phys. Rev. Lett. **104**, 046401 (2010).

[49] L. Fu and C. L. Kane, Time reversal polarization and a Z_2 adiabatic spin pump, Phys. Rev. B **74**, 195312 (2006).

[50] J. C. Y. Teo and C. L. Kane, Topological defects and gapless modes in insulators and superconductors, Phys. Rev. B **82**, 115120 (2010).

[51] D. Toniolo, Time-dependent topological systems: A study of the Bott index, Phys. Rev. B **98**, 235425 (2018).

[52] A. Y. Kitaev, Unpaired majorana fermions in quantum wires, Sov. Phys. Usp. **44**, 131 (2001).

[53] J. C. Budich and E. Ardonne, Equivalent topological invariants for one-dimensional majorana wires in symmetry class d, Phys. Rev. B **88**, 075419 (2013).

[54] J. C. Budich and E. Ardonne, Topological invariant for generic one-dimensional time-reversal-symmetric superconductors in class diii, Phys. Rev. B **88**, 134523 (2013).

[55] C. L. Kane and E. J. Mele, Quantum Spin Hall Effect in Graphene, Phys. Rev. Lett. **95**, 226801 (2005).

[56] F. D. M. Haldane, Model for a Quantum Hall Effect without Landau Levels: Condensed-Matter Realization of the "Parity Anomaly," Phys. Rev. Lett. **61**, 2015 (1988).

[57] I. Peschel, Calculation of reduced density matrices from correlation functions, J. Phys. A **36**, L205 (2003).

[58] A. S. Sørensen, E. Altman, M. Gullans, J. V. Porto, M. D. Lukin, and E. Demler, Adiabatic preparation of many-body states in optical lattices, Phys. Rev. A **81**, 061603 (2010).

[59] M. Barkeshli, N. Y. Yao, and C. R. Laumann, Continuous Preparation of a Fractional Chern Insulator, Phys. Rev. Lett. **115**, 026802 (2015).

[60] S. Diehl, E. Rico, M. A. Baranov, and P. Zoller, Topology by Dissipation in Atomic Quantum Wires, Nat. Phys. **7**, 971 (2011).

[61] J. C. Budich, P. Zoller, and S. Diehl, Dissipative preparation of chern insulators, Phys. Rev. A **91**, 042117 (2015).

[62] C. Nayak, S. H. Simon, A. Stern, M. Freedman, and S. Das Sarma, Non-abelian anyons and topological quantum computation, Rev. Mod. Phys. **80**, 1083 (2008).

[63] S. D. Sarma, M. Freedman, and C. Nayak, Majorana Zero Modes and Topological Quantum Computation, Quant. Info. **1**, 15001 (2015).

[64] J. Alicea, Y. Oreg, G. Refael, F. Von Oppen, and M. P. A. Fisher, Non-Abelian statistics and topological quantum information processing in 1D wire networks, Nat. Phys. **7**, 412 (2011).

[65] X.-J. Liu, C. L. M. Wong, and K. T. Law, Non-Abelian Majorana Doublets in Time-Reversal-Invariant Topological Superconductors, Phys. Rev. X **4**, 021018 (2014).

[66] K. Wölms, A. Stern, and K. Flensberg, Local Adiabatic Mixing of Kramers Pairs of Majorana Bound States, Phys. Rev. Lett. **113**, 246401 (2014).

[67] Y. Niu, S. B. Chung, C.-H. Hsu, I. Mandal, S. Raghu, and S. Chakravarty, Majorana zero modes in a quantum ising chain with longer-ranged interactions, Phys. Rev. B **85**, 035110 (2012).

[68] Despite the difference in symmetries of the two models, there is in fact a formal mapping between the six-Majorana system considered here and the one considered in Ref. [66], which means the Berry connections are equal if one replaces J in (14) with D in Eq. (6b) of Ref. [66].

[69] G. Goldstein and C. Chamon, Decay rates for topological memories encoded with majorana fermions, Phys. Rev. B **84**, 205109 (2011).

[70] G. Möller, N. R. Cooper, and V. Gurarie, Structure and consequences of vortex-core states in p-wave superfluids, Phys. Rev. B **83**, 014513 (2011).

[71] M. J. Schmidt, D. Rainis, and D. Loss, Decoherence of majorana qubits by noisy gates, Phys. Rev. B **86**, 085414 (2012).

[72] B. A. Bernevig, *Topological Insulators and Topological Superconductors* (Princeton University Press, Princeton, 2013).

[73] L. Mazza, M. Rizzi, M. D. Lukin, and J. I. Cirac, Robustness of quantum memories based on majorana zero modes, Phys. Rev. B **88**, 205142 (2013).

[74] This is valid as long as the Berry curvature at $\vec{\eta} = 0$ is nonzero, otherwise we should expand Ω to lowest nonzero order in $\vec{\eta}$. Although the fine-tuned 'ideal' models such as (13) have zero Berry curvature at the fine-tuned point, generic models including Hamiltonians (17) do have a nonzero Berry curvature.

[75] J. I. Väyrynen, D. I. Pikulin, and J. Alicea, Noise-Induced Backscattering in a Quantum Spin Hall Edge, Phys. Rev. Lett. **121**, 106601 (2018).